frontiers in Marine Science

ORIGINAL RESEARCH
published: 07 August 2019
doi: 10.3389/fmars.2019.00481

Non-conservative Behavior of Dissolved Organic Matter and Trace Metals (Mn, Fe, Ba) Driven by Porewater Exchange in a Subtropical Mangrove-Estuary

Corinna Mori[1], Isaac R. Santos[2,3], Hans-Jürgen Brumsack[1], Bernhard Schnetger[1], Thorsten Dittmar[1,4] and Michael Seidel[1]**

[1] Institute for Chemistry and Biology of the Marine Environment (ICBM), Carl von Ossietzky University of Oldenburg, Oldenburg, Germany, [2] National Marine Science Centre, Southern Cross University, Coffs Harbour, NSW, Australia, [3] Department of Marine Sciences, University of Gothenburg, Gothenburg, Sweden, [4] Helmholtz Institute for Functional Marine Biodiversity at the University of Oldenburg (HIFMB), Oldenburg, Germany

OPEN ACCESS

Edited by:
Sunil Kumar Singh,
Physical Research Laboratory, India

Reviewed by:
Gyana Ranjan Tripathy,
Indian Institute of Science Education and Research, Pune, India
Vineet Goswami,
Colorado State University, United States

***Correspondence:**
Corinna Mori
corinna.mori@uol.de
Michael Seidel
m.seidel@uol.de

Specialty section:
This article was submitted to Marine Biogeochemistry, a section of the journal Frontiers in Marine Science

Received: 12 April 2019
Accepted: 17 July 2019
Published: 07 August 2019

Citation:
Mori C, Santos IR, Brumsack H-J, Schnetger B, Dittmar T and Seidel M (2019) Non-conservative Behavior of Dissolved Organic Matter and Trace Metals (Mn, Fe, Ba) Driven by Porewater Exchange in a Subtropical Mangrove-Estuary. Front. Mar. Sci. 6:481. doi: 10.3389/fmars.2019.00481

Estuaries play a key role in controlling the land-ocean fluxes of dissolved organic matter (DOM), nutrients and trace metals. Here, we study how mangrove-fringed areas affect the molecular DOM and trace metal composition in a subtropical estuary. We combined molecular analysis of solid-phase extractable (SPE) DOM using ultrahigh-resolution mass spectrometry with organic and inorganic bulk parameter analyses in surface and porewater along the estuarine gradient of a mangrove-fringed estuary in Australia (Coffs Creek). Statistical analysis and mixing models demonstrate that the fluvial and mangrove-porewater derived DOM and inorganic chemical species were altered and/or removed by the estuarine filter before reaching the coastal ocean. The mangrove-fringed central estuary was a net source for dissolved Mn and Ba as well as total dissolved nitrogen (TDN) and dissolved organic carbon (DOC) to the tidal creek, likely due to the exchange of mangrove-porewater strongly enriched in these constituents. Dissolved Fe was removed from the water column, probably during the tidally driven circulation of creek water through the sulfidic mangrove sediments. In the mangrove-porewater dominated tidal creek, sulfur- and nitrogen-containing as well as aromatic DOM compounds were relatively enriched, whereas phosphorous-containing DOM was relatively depleted compared to non-mangrove fringed areas. In areas with intense mixing of estuarine and marine water masses we observed a strong decrease of these DOM compounds relative to values expected from conservative mixing, suggesting their removal by photodegradation and co-precipitation with particles such as Mn(hydr)oxides and/or as organometallic complexes, leading to more aliphatic DOM signatures at the creek-mouth. Tidally driven porewater exchange and surface water runoff from the mangroves had a stronger effect on the biogeochemical cycling in the estuary than the fluvial input during a dry compared to a wet season. Our study confirms that mangroves can significantly contribute to biogeochemical budgets of (sub)tropical estuaries.

Keywords: FT-ICR-MS, biogeochemical cycling, tidal pumping, flood events, small tidal creek, flux rates

INTRODUCTION

Estuarine ecosystems are major pathways for the export of dissolved organic matter (DOM) and inorganic constituents to the coastal ocean, where they often serve as nutrients for primary producers. Not only the large river/estuarine systems such as the Amazon (Medeiros et al., 2015; Seidel et al., 2015) are significant for coastal element budgets, but also small tidal creeks (Sanders et al., 2015). While there has been comprehensive research on DOM and trace metal cycling in the open ocean (Donat and Bruland, 1995; Hansell and Carlson, 2014) their dynamics in coastal systems (including estuaries and small tidal creeks) and the interaction with terrestrial systems and intertidal wetlands remain poorly understood.

The dissolved constituents of estuaries can be distinguished into allochthonous (from marine, riverine, atmospheric, and groundwater input) and autochthonous (from *in situ* primary production) materials. Submarine groundwater discharge (SGD), which includes fresh groundwater input and saline porewater exchange, can play a significant role in coastal element budgets (Moore, 2010). SGD is often enriched in DOM, nutrients and some trace metals compared to surface waters (e.g., Charette et al., 2005; Moore, 2010; Santos et al., 2011b; Maher et al., 2013; Reading et al., 2017). Several studies have shown that mangrove forests serve as biogeochemical reactors and play an active role in the decomposition of organic matter (Kristensen et al., 2008). They are also an important source for DOM (Bouillon et al., 2003, 2008; Dittmar et al., 2006), inorganic carbon (Sippo et al., 2016) and influence dissolved trace metals in the adjacent estuaries (Alongi et al., 1998; e Silva et al., 2006; Marchand et al., 2011; Holloway et al., 2016). It has been estimated that mangroves alone account for >10% of the flux of terrigenous DOM to the oceans, even though they cover <0.1% of the continents' surface (Dittmar et al., 2006). In urban areas, various anthropogenic activities such as discharge of sewage or increasing runoff due to deforestation, represents another important allochthonous source of DOM and trace metals in estuaries (Kennish, 1991).

Manganese (Mn) and iron (Fe) are redox sensitive elements, which are also essential micronutrients for primary production. In natural waters, Mn and Fe are either present in their oxidized, particulate form [Mn(IV, III), Fe(III)] or in their reduced dissolved form Mn(II) [or rarer Mn(III)], and Fe(II). Under euxinic conditions, dissolved Fe reacts rapidly with sulfides, forming insoluble phases as pyrite (FeS_2) and iron monosufildes (FeS) (Canfield, 1989). Both, Mn and Fe solid phases are known to scavenge a variety of trace elements as well as DOM either by surface adsorption, complexation or direct incorporation into the crystal structure (Burdige, 1993; Bruland and Lohan, 2003; Bauer and Bianchi, 2011). Under anoxic conditions, Mn and Fe oxides/hydroxides can serve as alternative electron acceptors for microbial processes (Froelich et al., 1979).

In coastal ocean studies, barium (Ba) is used as tracer for mixing as well as marine primary production (Coffey et al., 1997; Moore, 1997). Along estuarine transects, dissolved Ba concentrations can be controlled by various processes (Coffey et al., 1997), which include: (1) the mixing of water masses with different salinity and Ba concentrations (Coffey et al., 1997; Moore, 1997; Moore and Shaw, 2008; Santos et al., 2011a), (2) ion exchange driven adsorption/desorption processes to/from sediment and suspended particles (Hanor and Chan, 1977), (3) Fe- and Mn(hydr)oxide cycling (Coffey et al., 1997), and (4) biological precipitation (barite formation) and remineralization processes (e.g., Bishop, 1988; Stecher and Kogut, 1999).

DOM can be operationally divided into reactivity classes from labile to refractory (McKnight et al., 2001; Hansell et al., 2009; Bhatia et al., 2010; Schmidt et al., 2011). The traditional paradigm that vascular-plant derived polyphenols, such as lignin, are recalcitrant has been challenged because these phenols appear to be rapidly degraded by riverine microbes once they are in the dissolved phase (Ward et al., 2013). Degradation products of vascular polyphenols, often referred to as humic substances, represent a main fraction of terrestrial DOM. Due to their acidity and ability to absorb light as well as other properties, they can influence the physicochemical characteristic of natural water systems (Bhatia et al., 2010; Thurman, 2012).

Along estuarine gradients, DOM, nutrients and trace metals can be added, removed or modified due to a variety of complex biological, physical and chemical transformation and remineralization processes (Bauer and Bianchi, 2011). The main variables associated to these transformations are salinity (as a proxy for freshwater-seawater mixing), temperature, dissolved oxygen content (DO), pH as well as the type and concentration of suspended particles (Millward, 1995). Conservative mixing models along a salinity gradient are an established method for interpreting the sources and sinks of dissolved constituents in estuaries (Officer, 1979; Peterson et al., 1994). Because of complex and overlapping interactions, conservative mixing models alone do not constrain all potential sources (Peterson et al., 1994; Raymond and Bauer, 2001a; Fry, 2002). Molecular characterization of DOM, the stable carbon isotope ratios of dissolved organic carbon (δ^{13}C-DOC) and δ^{13}C mixing models also help to evaluate the fate of DOM along estuarine gradients (Spiker, 1980; Peterson et al., 1994; Raymond and Bauer, 2001b; Tremblay et al., 2007). However, due to overlaps of isotopic signatures of the major dissolved organic carbon (DOC) sources in estuaries, the interpretation of δ^{13}C-DOC can be hampered (Raymond and Bauer, 2001a). The combined application of conservative mixing models, δ^{13}C-DOC and molecular characterization of the DOM composition has the potential to improve our understanding of the distribution, transformation and fate of estuarine DOM (Dittmar et al., 2001).

The molecular characterization of solid-phase extractable (SPE) DOM via ultrahigh-resolution Fourier-transform ion cyclotron resonance mass spectrometry (FT-ICR-MS) yields thousands of molecular formulae in the complex DOM mixture. Hence, FT-ICR-MS is a strong tool to investigate DOM processing in estuaries (Tremblay et al., 2007; Sleighter and Hatcher, 2008; Seidel et al., 2015; Osterholz et al., 2016). The transformation processes of terrestrial and the autochthonous production of DOM are not necessarily reflected by changes in bulk DOC concentrations. However, transformation processes leave characteristic imprints in the DOM molecular

composition. For instance, the decrease of aromatic terrestrial DOM-compounds along a salinity gradient or the enrichment of sulfur-containing compounds along different redox-regimes (Seidel et al., 2014; Medeiros et al., 2015; Osterholz et al., 2016; Pohlabeln et al., 2017).

This study investigates processes affecting the molecular DOM composition as well as dissolved Mn, Fe, and Ba concentrations and distribution in a subtropical, mangrove-dominated, urban estuary during a wet and a dry season. Previous studies based on short-lived radium (Ra) and radon (Rn) isotopes revealed that the greenhouse gas dynamics in the area (Coffs Creek Estuary, Australia) are closely related to tidally driven saline porewater exchange in mangrove crab burrows (Reading et al., 2017; Sadat-Noori et al., 2017; Jeffrey et al., 2018). In this study we address how mangroves modify the molecular DOM composition and affect trace metal dynamics from the estuary into the ocean. We hypothesize that, (1) the estuary is a source of terrestrial DOM and dissolved trace metals (Mn, Fe, and Ba) to the coastal ocean, (2) the estuarine DOM reservoir is dominated by terrestrial organic matter from the catchment area and that (3) changing discharge conditions (dry vs. wet season) as well as coupled runoff, porewater exchange and groundwater input affect the DOM and trace metal distributions. To address these hypotheses, we compared DOC concentrations, δ^{13}C-DOC, the molecular composition of DOM and Mn, Fe as well as Ba distributions in surface waters along the estuarine gradient before and after a heavy rain event as well as saline pore- and deep fresh groundwater samples.

MATERIALS AND METHODS

Study Site

The study area is Coffs Creek Estuary, a subtropical, wave dominated estuary in Coffs Harbour, Australia (**Figure 1**). The catchment covers an area of 24.5 km^2, with an estimated population of 18,000 people (Roper et al., 2011). It is characterized by steep and highly erodible hillsides and contains a wide variety of ecosystems, such as forests, wetland, saltmarsh, and mangroves (Milford, 1999). More than 80% of the catchment area is dominated by urban development and agriculture, while ∼16% are considered undisturbed (Roper et al., 2011). The annual precipitation averages 1,699 mm year^{-1}, with the wettest month being February and the driest month being September (GeoLINK, 2013). The semidiurnal tidal range is up to 1.85 m. Flow speed during incoming tide ranges from 0.1 m s^{-1} upstream to 1.0 m s^{-1} at the mouth. Coffs Creek Estuary is well-mixed and the water body is completely flushed over four tidal cycles (Water Technology, 2013). Based upon previously published characteristics such as depositional processes, hydrology, sediment sources and textures, four main zones along the estuary can be distinguished (GeoLINK, 2013; Sadat-Noori et al., 2017): (1) Marine (Stations 1–3), (2) Mangrove-fringed (Stations 4–10), (3) Fluvial-mangrove transition (Stations 11–15), and (4) Fluvial (Stations 16–18) (**Figure 1** and **Supplementary Table S1**).

Sampling

Sampling at Coffs Creek Estuary consisted of two aspects: (1) the determination of the spatial distribution of the DOM molecular composition and trace metals (dissolved Mn, Fe, and Ba) in surface waters of the estuary during a dry and a wet season, in order to assess the influence of a precipitation event (>45 mm in 24 h) and (2) an assessment of fresh groundwater discharge and saline porewater exchange as potential sources and sinks of DOM and trace metals.

The first survey was conducted on March 1st, 2016 after a dry period of approximately three weeks with just 3.8 mm precipitation. Usually, March is one of the wettest months in this region, but El Niño conditions caused a drought. The second survey was conducted on April 14th, 2016, one day after a heavy rain event (49.1 mm). Samples were collected from surface waters (∼10 cm depth), using a sample rinsed polyethylene syringe (60 mL), connected to polyethylene tubing. All surface water samples in the tidally influenced part of the estuary were taken during flood tide, starting from Station 1 at the mouth and following the creek upstream toward Station 18 (**Figure 1** and **Supplementary Table S1**). Sampling was conducted during normal tidal conditions, i.e., between spring and neap tide cycles, with a tidal range of ∼0.5 to 1.5 m at low and high tide, respectively.

Porewater samples were taken during the March 2016 campaign at four different locations along the salinity gradient (**Figure 1** and **Supplementary Table S2**). To characterize the deep fresh groundwater endmember, an additional sample from a deep well ("W" in **Figure 1**, 28 m deep) was taken. Porewater samples at each location (A–D), were taken during low tide, from one-meter bores along transects and from low- to high-tide mark. PVC pipes with 50 cm long screens were installed to retrieve porewater samples after the wells were flushed completely three times. While this sampling approach does not allow for resolving biogeochemical processes within intertidal groundwater, it provides insight into the endmember concentration of porewaters exchanging with the estuary (Santos et al., 2014).

Samples for the determination of DOC and TDN concentrations, molecular DOM composition and δ^{13}C-DOC were filtered through pre-combusted (400°C, 4 h), sample rinsed (∼5 mL) 0.7 μm Whatman GF/F filters into acid-rinsed (HCl), ultrapure water-washed, pre-combusted (450°C, 4 h) 40 mL volatile organic carbon (VOC) borosilicate vials. The vials contained three drops of H_3PO_4 (85%) to remove dissolved inorganic carbon, leaving a headspace for degassing. DOM samples were filtered into acid-rinsed, ultrapure water washed polycarbonate bottles (Nalgene, 500 mL). Samples for trace metal analysis were immediately filtered in-field through sample-rinsed disposable 0.45 μm SFCA (surfactant-free cellulose acetate) syringe filters into 10 mL, acid-cleaned, and sample-rinsed, polypropylene vials. All samples were stored on ice, in the dark until further treatment. Trace metal samples were acidified using concentrated ultrapure HNO_3 to obtain a concentration of 1% (v/v). Procedural blanks with ultrapure water for all examined molecular and bulk parameters were treated the same way as

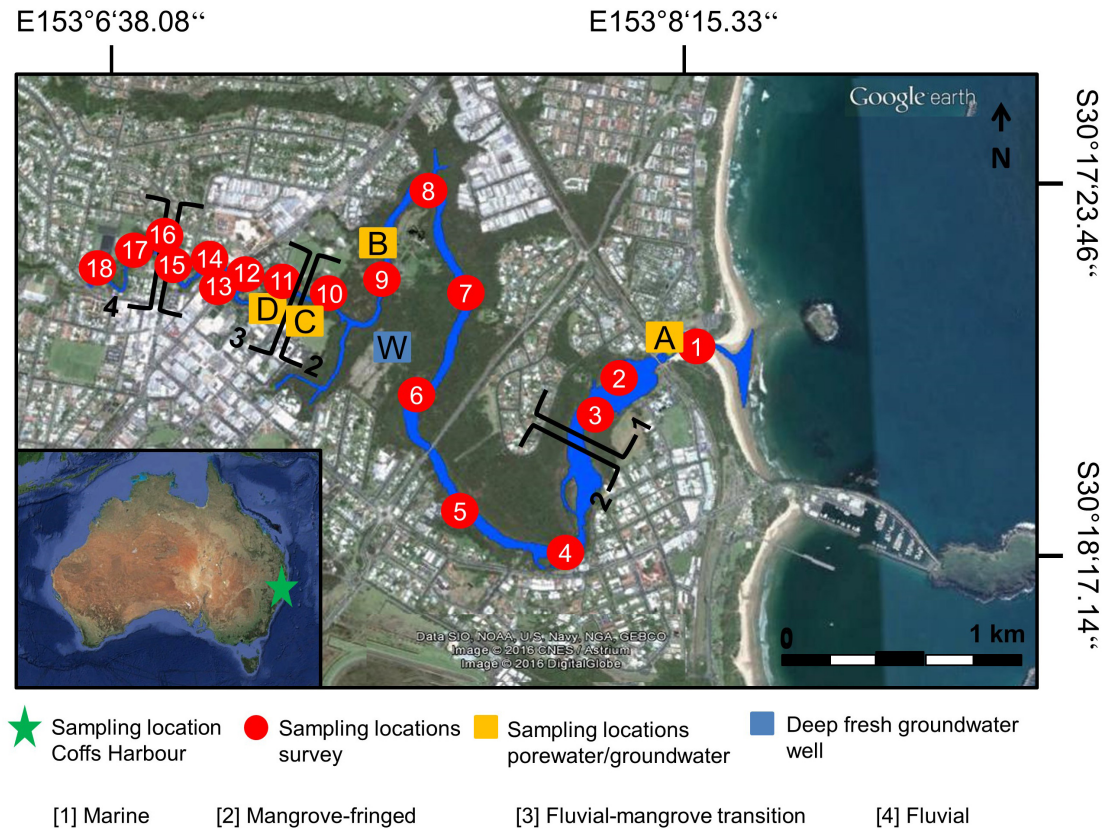

FIGURE 1 | Sampling location Coffs Creek Estuary in Coffs Harbour, NSW, Australia (green star); source maps ©2016 Google earth. Red numbered circles represent sampling locations for surface water samples (dry and wet season). Yellow squares with capital letters represent locations where porewater samples were taken. The blue square shows the location of 28-m deep fresh groundwater well. Numbers [1]–[4] divide the estuarine transect into four main zones: [1] marine, [2] mangrove-fringed, [3] fluvial-mangrove transition, and [4] fluvial zone.

natural water samples during sampling and analysis. During the dry season (March), we installed Acoustic Doppler Current Profilers (SonTek Argonaut XR at site A–D) and an ultrasonic Doppler instrument (Unidata Starflow 6526) at station 18 to capture average water velocities, in the different sections of the estuary, over a period of 25 h, covering two complete tidal cycles (**Figure 1**).

Bulk Biogeochemical Analyses

Salinity (±0.2), water temperature (±2°C), pH (±0.002), and DO (±0.1 mgL^{-1}) were determined in situ using pre-calibrated multi-parameter probes (EcoSense EC300A and Hach HQ40d). DOC and δ^{13}C-DOC were analyzed with the continuous flow wet oxidation method (St-Jean, 2003) using an OI Aurora 1030W coupled with a Thermo Delta V+ Isotope Ratio Mass Spectrometer (irMS). Carbon isotopic ratios (δ^{13}C) are expressed in delta notation, calculated relative to the international standard Vienna Pee Dee Belemnite. Trueness and precision for DOC and δ^{13}C-DOC were better than 4% and 0.8‰, respectively (Maher and Eyre, 2011) and the DOC detection limit was 33 µmol L^{-1}. TDN concentrations (includes nitrogen oxides NO_x, ammonium NH_4^+, dissolved organic nitrogen DON), and inorganic ortho-phosphate (PO_4^{3-}) were analyzed by flow injection analysis (Lachat Quikchem 8000 Flow Injection Analyzer) (Lachat, 1994) with a detection limit of 0.07 µmol L^{-1} and a precision better than 3.6%.

Mn, Fe, and Ba were analyzed using inductively coupled plasma mass spectrometry (ICP-MS) (Element 2, Finnigan MAT). Saline samples were diluted to a salinity of 2 (with 2% v/v ultrapure HNO_3) and freshwater samples were measured undiluted. The salinity-dependent limit of quantification for Mn, Fe and Ba was better than 0.03 µmol L^{-1}, 0.07 µmol L^{-1}, and 27 nmol L^{-1}, respectively (**Supplementary Table S3**). Samples below the limit of quantification were set to zero. Reference samples of spiked CASS-5 and NASS-6 for saline samples, SLEW-4 for estuarine samples and SLRS-3 for freshwater samples (National Research Council of Canada) were used to monitor trueness and precision (Menditto et al., 2007). Replicate measurements showed that trueness and precision were better than 10 and 5%, respectively (**Supplementary Table S4**).

Molecular DOM Analysis

DOM was extracted from filtered and acidified (HCl analytical grade, pH 2) surface water samples using SPE on styrene divinyl benzene polymer filled cartridges (Agilent Bond Elut PPL, 100 mg) according to Dittmar et al. (2008). To avoid

overloading the cartridges, we extracted a volume of 50 mL per sample (max. 20 μmol DOC). DOM was eluted with methanol after desalting the cartridge with 0.01 M HCl (analytical grade). The methanol extracts were stored frozen (−20°C) in the dark until analysis. The extraction efficiencies were calculated as DOC concentration in SPE-DOC versus concentration in the corresponding water sample. The SPE-DOC concentration was determined by drying an aliquot of the methanol extract (SPE-DOM) at 40°C and re-dissolving it in ultrapure water.

For the molecular characterization of DOM with FT-ICR-MS (15 Tesla solariX, Bruker Daltonik), methanol extracts were diluted with ultrapure water and methanol (HPLC grade, Sigma Aldrich) to yield a SPE-DOC concentration of 10 mgC L^{-1} and a methanol to water ratio of 1:1 (v/v). The methanol-water-mixtures were infused with a flow rate of 2 μL min^{-1} with a capillary voltage set on 4.5 kV and electrospray ionization (ESI) in negative mode. Negatively charged ions were accumulated for 0.1 s in the hexapole and data were recorded in broadband mode using 8 megaword data sets and a scan-range of 115.2–2,000 Da per mass spectrum. For each run, 200 broadband scans were accumulated. All samples (n = 32, including process blanks) were analyzed in a random order. To determine instrument variability during the measurement, a lab-intern reference material [n = 4, SPE-DOM from North Equatorial Pacific Intermediate Water, see Green et al. (2014) for details] was measured at the beginning and the end of each run. Each mass spectrum was internally calibrated with a reference mass list of compounds covering the targeted mass range (achieved mass accuracy <0.1 ppm). Molecular formulae were assigned to the detected mass peaks with a signal-to-noise ratio >4 applying the restrictions described in Rossel et al. (2013). The FT-ICR-MS signal intensity of each detected mass with an assigned molecular formula was normalized to the sum of intensities of all masses with assigned molecular formulae in each sample and multiplied by a factor of 1,000.

Weighted averages of the number of carbon (C), hydrogen (H), oxygen (O), nitrogen (N), sulfur (S), and phosphorous (P) atoms, molar ratios of H/C and O/C as well as AI_{mod}, which is a parameter developed to identify aromatic and condensed aromatic structures in DOM molecular formulae (Koch and Dittmar, 2006, 2016), were calculated for each sample (Seidel et al., 2014). The molecular compound groups, i.e., g1: polycyclic aromatic, g2: highly aromatic, g3: highly unsaturated, g4: unsaturated aliphatic, g5: saturated compounds with low O/C ratios, which may include lipids, g6: saturated compounds with high O/C ratios, which may include carbohydrates, and g7: unsaturated aliphatic compounds containing nitrogen were assigned to the molecular formulae as described in Seidel et al. (2017). These compound group assignments can provide information about the possible structure of the molecular formulae and it is a valuable tool to identify biogeochemical drivers of the DOM composition (e.g., Medeiros et al., 2015; Osterholz et al., 2016; Seidel et al., 2017). However, each assigned molecular formula may consist of many structural isomers (Zark et al., 2017). Hence, this categorization does not necessarily indicate the presence of a structural entity.

Statistical Analysis

To compare the molecular composition of the samples, we performed a principal coordinate analysis (PCoA) on a Bray–Curtis dissimilarity matrix of the normalized signal intensities of the detected DOM molecular formulae. In general, PCoA produces uncorrelated axes which summarize the variability within the dataset (Ramette, 2007). Each of the generated explaining axis has an eigenvalue which indicates the amount of variation displayed by it. Instead of eigenvalues, we calculated the proportion of a given eigenvalue to the sum of all eigenvalues. This reveals the relative importance (in percent) of each axis. Each station is given a score along each axis, which provides the coordinates of the stations in the ordination plot. Their spatial arrangement displays how similar the DOM molecular composition of different stations is compared to each other. Sites plotting close to each other have similar DOM molecular compositions whereas sites that are more separated are more dissimilar. PCoA aims to identify most of the variance in the DOM molecular composition and allows to describe relationships among different sites along the estuarine transect, based on the first two major axes of variation. To identify the endmembers within the DOM pool, we used a Ward's hierarchical clustering based on the Bray–Curtis dissimilarity matrix. The significant DOM compound groups, intensity-weighted averages of DOM parameters and environmental data were fitted to the PCoA scores using the *envfit* function provided by the *vegan* package (Oksanen et al., 2015) using R (version 3.4.1, R Core Team, 2016). The correlation of the DOM molecular composition and environmental parameters were tested with 10,000 permutations and was considered significant if $p \leq 0.1$. In the PCoA plots, the projections of sampling points onto the vectors of the DOM molecular compound groups and environmental parameters depict correlations with the corresponding parameters. To assess the linear relationship between DOM compounds and environmental parameters, Pearson correlation was used. This analysis allows to identify gradients in DOM molecular composition with respect to significantly correlated and thus potential environmental drivers. Based on duplicate and replicate FT-ICR-MS measurements, we found a reproducibility of the peak detection and molecular formula assignment procedures of better than 80%. All Van Krevelen plots were produced using the Ocean Data View software (Schlitzer, 2002).

Mixing Models and Flux Calculations

To assess how the concentrations of Mn, Fe, Ba, DOC, and TDN as well as δ^{13}C-DOC deviated from values expected from conservative mixing along the estuarine gradient, we applied linear regression analyses. In the following we use the term "bulk parameters" for this group of compounds. The deviation of DOM compound groups and bulk parameters from conservative mixing (Δ_{mix}) was calculated as described in Seidel et al. (2017). The calculated Δ_{mix} values indicate the difference between the theoretical conservative mixing and the actual measured concentration for bulk parameters and the scaled DOM compound groups. The DOM compound groups were

scaled by multiplying the relative abundance of each compound group to the DOC concentration before normalizing the data to values between 0 (minimum) and 1 (maximum). All surface and porewater plots were produced using Ocean Data View 4 (Schlitzer, 2002).

We further estimated the deviations of the concentrations of all compounds from conservative mixing in the four different zones along the estuarine transect to evaluate the influence of potential sources and sinks in the respective area. By multiplying the measured bulk concentrations of the freshwater, riverine endmember (C_{fw}) and the average discharge rate at the fluvial endmember site (S18) over a complete tidal cycle (25 h), we estimated the riverine fluxes of organic and inorganic matter toward the estuary. In order to quantify fluxes from the estuary into the ocean, we further calculated the effective freshwater concentration (C^*_{fw}) that reflects fluxes into the ocean after all biogeochemical processes took place within the estuary (Kaul and Froelich, 1984; Santos et al., 2009). For the calculation of the effective freshwater endmember C^*_{fw}, we estimated the zero-salinity intercept using the linear regression between solute and salinity for the downstream sites S1–S9.

RESULTS

General Observations in the Surface Water

Surface water salinities during dry and wet season were highest in the marine and lowest in the fluvial zone (**Figure 2** and **Supplementary Table S5**). Note that some water samples have higher than seawater salinity, but this is not uncommon in Australian estuaries due to evapotranspiration within mangroves (Reading et al., 2017). A three week-long drought and extensive evaporation prior to the dry season sampling led to very high salinities in surface as well as in shallow pore waters (see section "Biogeochemical Parameters: Pore- and Groundwater Observations"). Highest surface water temperatures during dry season around 29°C were observed in the mangrove-fringed zone and lowest values around 25°C in the fluvial zone. During wet season, lowest temperatures of 21°C were found in the fluvial zone, while highest values of 26°C were observed at the marine endmember. In general, we observed lower temperatures after the heavy rain event. Surface water pH during the dry season ranged from 7.8 in the marine zone to 6.5 in the fluvial and fluvial-mangrove transition zones. During the wet season, pH values ranged from 8.2 in the marine zone to 6.9 in the mangrove endmember and in the fluvial-mangrove transition zone (**Figure 2**).

Dissolved Trace Metals

Highest dissolved Mn concentrations during the dry season of 9.3 μmol L^{-1} were observed in the mangrove endmember (S10), while lowest concentrations were found in the freshwater (S18) and marine (S1) endmember. During the wet season, Mn concentrations were generally lower (0.1 μmol L^{-1} at S1 to 4.4 μmol L^{-1} at S12) (**Figure 3d**).

Dissolved Fe concentrations during the dry season were highest (2.1 μmol L^{-1}) in the freshwater endmember but showed a significant drop when entering the fluvial-mangrove transition zone (**Figure 2e**). During the wet season, dissolved Fe concentrations were generally higher but had similar distribution patterns compared to the dry season with highest concentrations of 6.6 μmol L^{-1} in the fluvial zone followed by a rapid drop when entering the mangrove-fringed zone (S10). Dissolved Fe concentrations in the marine endmember were below limit of determination and set to 0 μmol L^{-1} in both seasons.

Highest dissolved Ba concentrations (360 nmol L^{-1}) in the dry season were found in the fluvial zone decreasing along the mangrove-fringed zone toward the marine endmember (60 nmol L^{-1}, **Figure 2f**). During the wet season, Ba concentrations were generally lower than during the dry season (112 to 153 nmol L^{-1} from S18 to S14), and they increased between S13 and S10 to 167 nmol L^{-1}. Again, concentrations decreased along the mangrove-fringed zone and lowest values of 50 nmol L^{-1} were found in the marine endmember (S1).

All observed dissolved trace metals (Mn, Fe, and Ba) showed non-conservative behavior along the estuarine/salinity gradient (**Figure 4**). Strongest positive (Mn, Ba) and negative (Fe) deviations from conservative mixing of the fluvial and marine endmembers during the dry season were observed in the central estuary. During the wet season, we found a similar pattern with a stronger influence of freshwater inputs overprinting the mangrove-porewater signal.

DOC, δ^{13}C-DOC, and TDN

During the dry season, highest surface water DOC concentrations (up to 353 μmol L^{-1}) were found in the fluvial- and central mangrove-fringed zone, with decreasing concentrations toward the marine endmember (100 μmol L^{-1}, **Figure 2h**). Higher DOC concentrations (up to 430 μmol L^{-1}) between the fluvial- (S18) and mangrove (S10) endmembers with a distribution patterns comparable to the dry season were observed during the wet season (**Figure 3h**).

Values for δ^{13}C-DOC along the transect during the dry season ranged from −16.2‰ (S1) in the marine zone to −27.0‰ (S15-S18) in fluvial- and mangrove-fringed transition zone (**Figure 2i**). While δ^{13}C-DOC values for the marine- and mangrove-fringed zone were comparable for both seasons, a more ^{13}C-enriched DOC signal was found in the fluvial zone during the wet season compared to the dry season (**Figure 3i**).

Surface water TDN concentrations during the dry season ranged from 29.6 μmol L^{-1} (S12) in the fluvial-mangrove transition zone to 7.4 μmol L^{-1} in the marine endmember (**Figure 2j**). During the wet season, highest values of 75.0 μmol L^{-1} were found at the mangrove endmember station (S10), while lowest values of 15.0 μmol L^{-1} were present at S2 in the marine zone (**Figure 3j**).

In the dry season, the sulfur-containing DOM compounds were enriched in the mangrove-fringed zone (**Figure 2g**). In the wet season, sulfur-containing DOM compounds were relatively enriched in the fluvial zone and decreased toward the marine endmember (**Figure 3g**). Phosphorous-containing DOM compounds were relatively depleted in the fluvial zone and

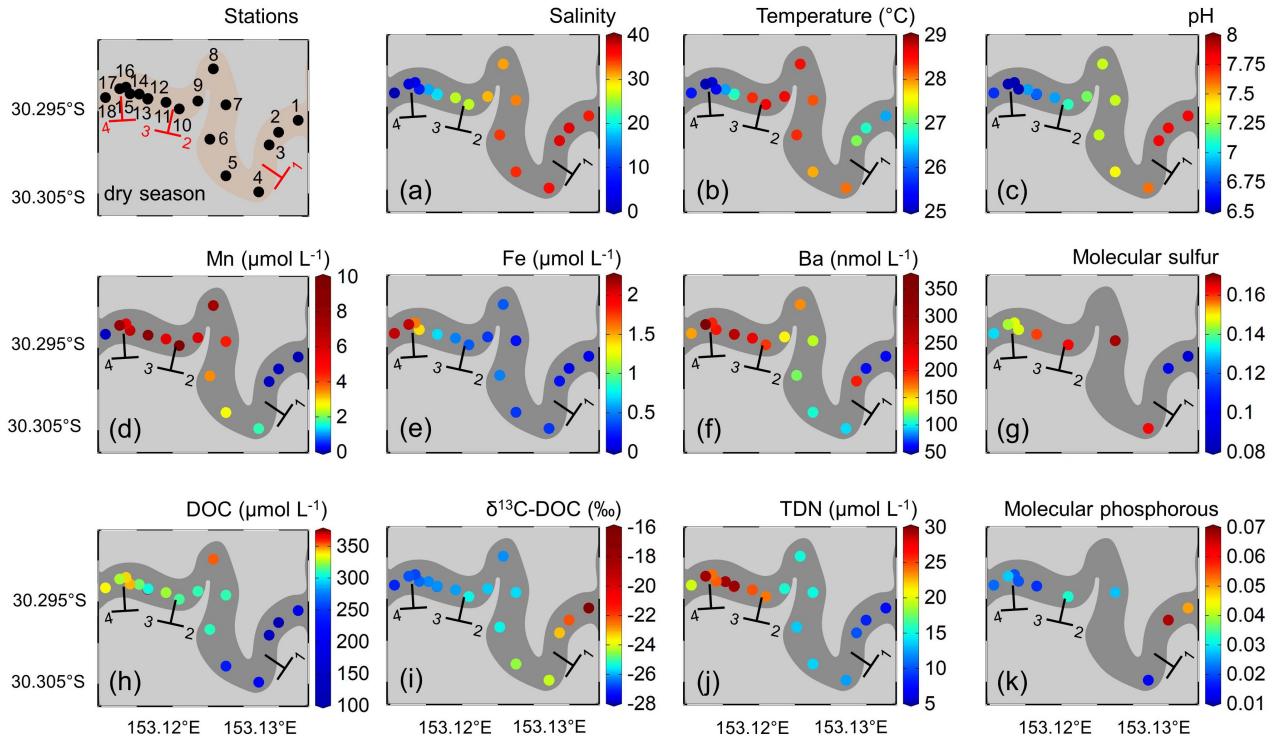

FIGURE 2 | Surface water properties along the estuarine transect during the dry season with **(a)** salinity, **(b)** temperature (°C), **(c)** pH, **(d)** dissolved manganese (Mn) (μmol L^{-1}), **(e)** dissolved iron (Fe) (μmol L^{-1}), **(f)** dissolved barium (Ba) (nmol L^{-1}), **(g)** intensity-weighted averages of DOM molecular sulfur, **(h)** dissolved organic carbon (DOC) (μmol L^{-1}), **(i)** dissolved organic carbon isotopic composition (δ^{13}C-DOC) (‰), **(j)** total dissolved nitrogen (TDN) (μmol L^{-1}), and **(k)** intensity-weighted average of DOM molecular phosphorous along the estuarine transect of Coffs Creek estuary. The different zones along the estuarine transect are labeled according to **Figure 1**.

increased toward the marine endmember in the wet and the dry season (**Figures 2k**, **3k**).

The mixing plots show a non-conservative behavior for DOC, δ^{13}C-DOC, and TDN along the estuarine transect during both seasons (**Figure 4**). Note that the conservative mixing of δ^{13}C-DOC values appears curved (non-linear) despite the linear mixing of water masses as it involves the mixing of isotopic ratios. The strongest deviation from the conservative mixing trend was observed in the central part of the estuary during the dry season and in the fluvial zone during the wet season (**Figure 4**).

Biogeochemical Parameters: Pore- and Groundwater Observations

Pore- and groundwaters were separated according to depth into: (1) shallow (≤0.5 m), (2) medium (0.5–3.0 m), and (3) deep (W = 28 m) stations (**Figure 5**). Salinities ranged from 38 in shallow porewaters at station A to zero in the deep groundwater at station W (**Figure 5A**). Highest porewater temperatures of up to 29°C were observed in the shallow porewaters at station A and lowest values of 22°C in the shallow porewaters at station D, medium porewaters at station C and in the deep groundwater endmember (W) (**Figure 5B**). Highest pH values of 7.4 were found in shallow porewaters at station A and lowest values of 4.2 in medium porewaters at station C (**Figure 5C**).

Lowest DOC concentrations of 50 μmol L^{-1} were found in the deep groundwater endmember (W). While the shallow porewaters showed similar concentrations to surface waters, highest DOC concentrations of 1,796 μmol L^{-1} and up to 3,410 μmol L^{-1} were observed in the medium porewaters at station B to D (**Figure 5D**). Values of δ^{13}C-DOC ranged between −22‰ in shallow porewaters at station A and −25‰ to −27‰ in the porewaters at station B to D and in the deep groundwater endmember (**Figure 5E**). TDN concentrations were highest in porewaters of the fluvial-mangrove transition zone, with highest values of 712 μmol L^{-1} in medium depths porewaters at station D. Lowest concentrations (<100 μmol L^{-1}) were found in porewaters from station A and B (**Figure 5F**). Highest PO_4 concentrations were observed in the medium (12.6 μmol L^{-1}) and shallow porewaters (7.9 μmol L^{-1}) at station D. PO_4 concentrations in porewaters at station C, B, and A were <1 μmol L^{-1} (**Figure 5G**).

Mn concentrations ranged from 24.0 μmol L^{-1} in medium porewaters at station B to 0 μmol L^{-1} in the deep groundwater endmember (W) (**Figure 5H**) and were twice as high as in surface waters. Highest dissolved Fe concentrations of 101 μmol L^{-1} were found in medium porewater at station B and lowest concentrations of 0.5 μmol L^{-1} in the shallow porewaters at station A (**Figure 5I**). Fe concentrations in porewater were up to 50 times higher compared to surface waters. Ba concentrations

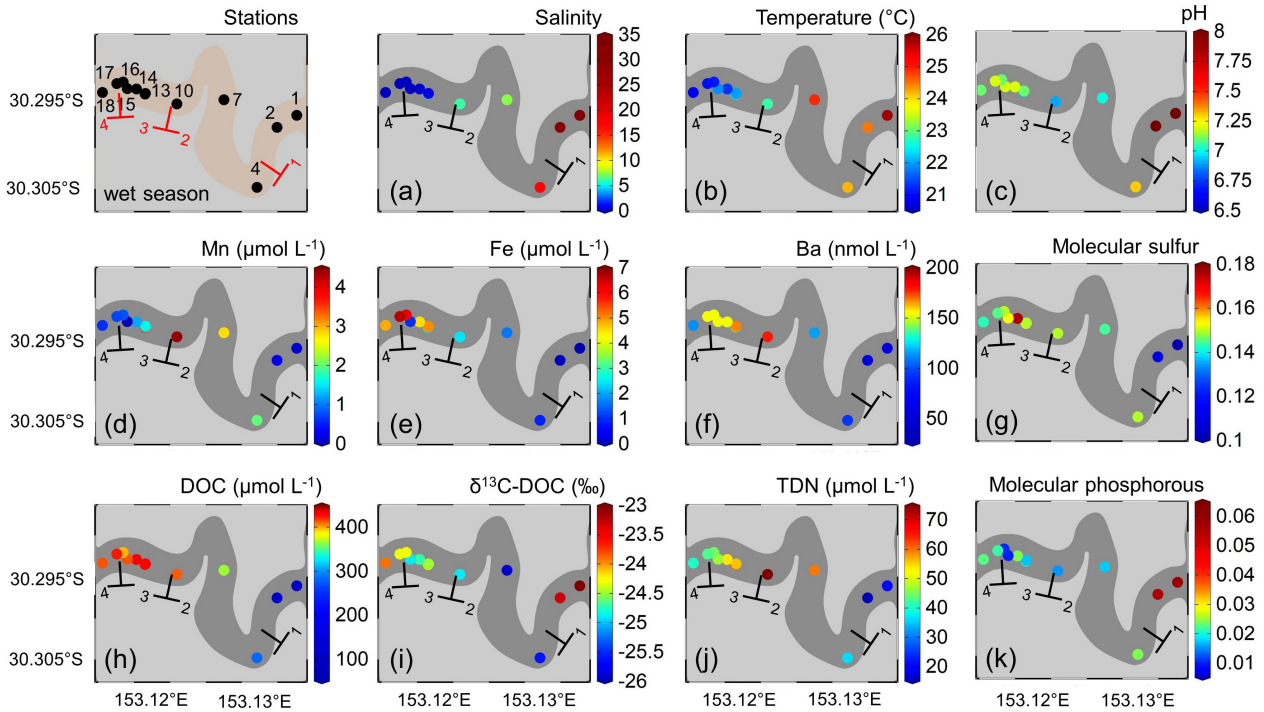

FIGURE 3 | Surface water properties along the estuarine transect during the wet season of **(a)** salinity, **(b)** temperature (°C), **(c)** pH, **(d)** dissolved manganese (Mn) (μmol L^{-1}), **(e)** dissolved iron (Fe) (μmol L^{-1}), **(f)** dissolved barium (Ba) (nmol L^{-1}), **(g)** intensity-weighted average of DOM molecular sulfur, **(h)** dissolved organic carbon (DOC) (μmol L^{-1}), **(i)** dissolved organic carbon isotopic composition (δ^{13}C-DOC) (‰), **(j)** total dissolved nitrogen (TDN) (μmol L^{-1}), and **(k)** intensity-weighted average of DOM molecular phosphorous along the estuarine transect of Coffs Creek estuary. The different zones along the estuarine transect are labeled according to **Figure 1**.

in porewaters were up to 10 times higher than surface waters, especially in the fluvial-mangrove transition and mangrove-fringed zone, ranging from 3,970 nmol L^{-1} in the medium porewaters at station D to 190 nmol L^{-1} in the shallow porewaters at station A (**Figure 5J**). The highest DO saturation was found at station D in a depth of 3 m. The DO saturation was lowest in the shallower porewaters at the same site (**Figure 5K**).

DOM – Molecular Characterization

In 28 SPE-DOM samples, 16,482 unique molecular formulae in the mass range of 120–850 Da, were identified. Extraction efficiencies were 45 ± 7% (n = 32) on a carbon basis and uncorrelated to salinity, which demonstrates that there was no preferential extraction of marine over terrestrial DOM.

During the dry season, the highest number of unique molecular formulae (n = 274; only present in this respective sample set) was identified in the mangrove and lowest (n = 30) in the fluvial endmember (**Table 1**). During the wet season, the number of unique molecular formulae of the endmembers ranged between 324 (marine) and 267 (fluvial). During the dry season, the weighted-average molecular masses increased from the fluvial to the marine endmember. The highest weighted-average AI_{mod} values were found in the fluvial compared to the mangrove and marine endmembers. During the dry season, the marine endmember was considerably enriched in aromatic compounds compared to the wet season. During the dry season, the weighted-average values of N were highest in the marine endmembers, whereas weighted-average N was highest in the mangrove endmember samples in the wet season.

During the dry season, values of DOC-concentration-scaled relative abundances of unsaturated aliphatics containing N (g7) were lowest in freshwater and highest in the mangrove-marine transition zone (**Figure 4** and **Supplementary Tables S5–S7**). All DOC-concentration-scaled abundances, especially those located in the mangrove-fringed zone, were higher than values expected from conservative mixing indicating a source within the mangroves. The DOC-scaled relative abundances of nitrogen-, sulfur- and phosphorous-containing DOM as well as polycyclic aromatic (g1), highly aromatic (g2), highly unsaturated (g3), unsaturated aliphatic (g4), saturated compounds with low O/C ratios (g5), and saturated with high O/C ratios (g6) molecular components showed the opposite trend, with highest values in the freshwater and lowest values in the marine endmember (**Figure 4** and **Supplementary Figure S1**). In the fluvial-mangrove transition and porewater-mangrove zone, all DOC-scaled abundances, except for phosphorous-containing DOM, were above values expected from conservative mixing, indicating a source for these compounds in this area. The DOC-scaled relative abundances of phosphorous-containing DOM were more scattered, but they were overall below values expected from conservative mixing, suggesting removal along the transect.

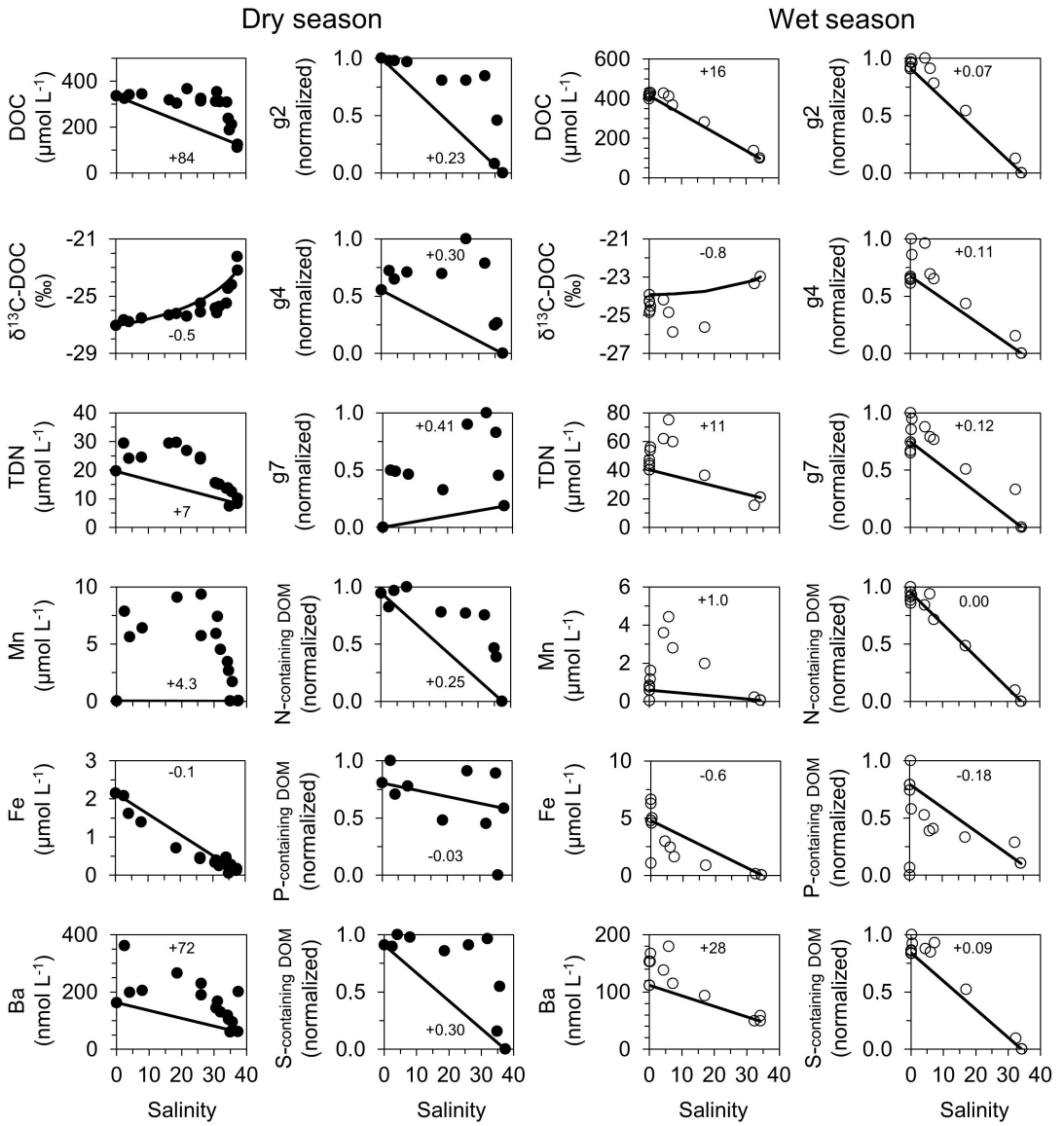

FIGURE 4 | Conservative mixing plots of bulk and molecular DOM surface water parameters. Left panels (•) represent the dry season, right panels (○) represent the wet season. Note different scales for bulk parameters between dry and wet seasons. The error bars for DOC, δ^{13}C-DOC, TDN, Mn, Fe, and Ba are not visible as the size of the symbols exceeds the respective errors. Solid black lines indicate the theoretical conservative mixing line between freshwater and marine endmember of bulk parameters: DOC (µmol L^{-1}), δ^{13}C-DOC (‰), TDN (µmol L^{-1}), Mn (µmol L^{-1}), Fe (µmol L^{-1}), Ba (nmol L^{-1}); the relative abundance of DOM compound groups and components: highly aromatic (g2), unsaturated aliphatic (g4), aliphatic compounds containing N (g7), nitrogen-, phosphorous-, sulfur-containing DOM. The relative abundances of the DOM compound groups were scaled to the DOC concentrations and normalized to their minimum and maximum values. In-box numbers indicate whether Coffs Creek estuary is a relative source (+) or sink (–) for the respective parameter. Note that for δ^{13}C-DOC conservative mixing results in a non-linear relationship with salinity.

During the wet season, the overall distribution patterns of DOC-concentration-scaled relative abundances of DOM molecular compound groups were more dominated by inputs from the freshwater endmembers (highest relative abundance in freshwater endmembers, **Figure 4**) compared to the dry season. All DOC-scaled relative abundances of DOM groups, except for phosphorous-containing DOM, showed less deviation from values expected from conservative mixing compared with highest relative abundances in freshwater DOM and lowest in the marine endmember (**Figure 4** and **Supplementary Figure S1**).

Statistical Analysis

The DOM molecular patterns were analyzed by PCoA, performed on a Bray–Curtis dissimilarity matrix (**Figure 6**). During both seasons, the first two axes explained >80% of the variability within the complex DOM mixtures. Based on our observations we subdivided the stations into three main groups: (1) marine,

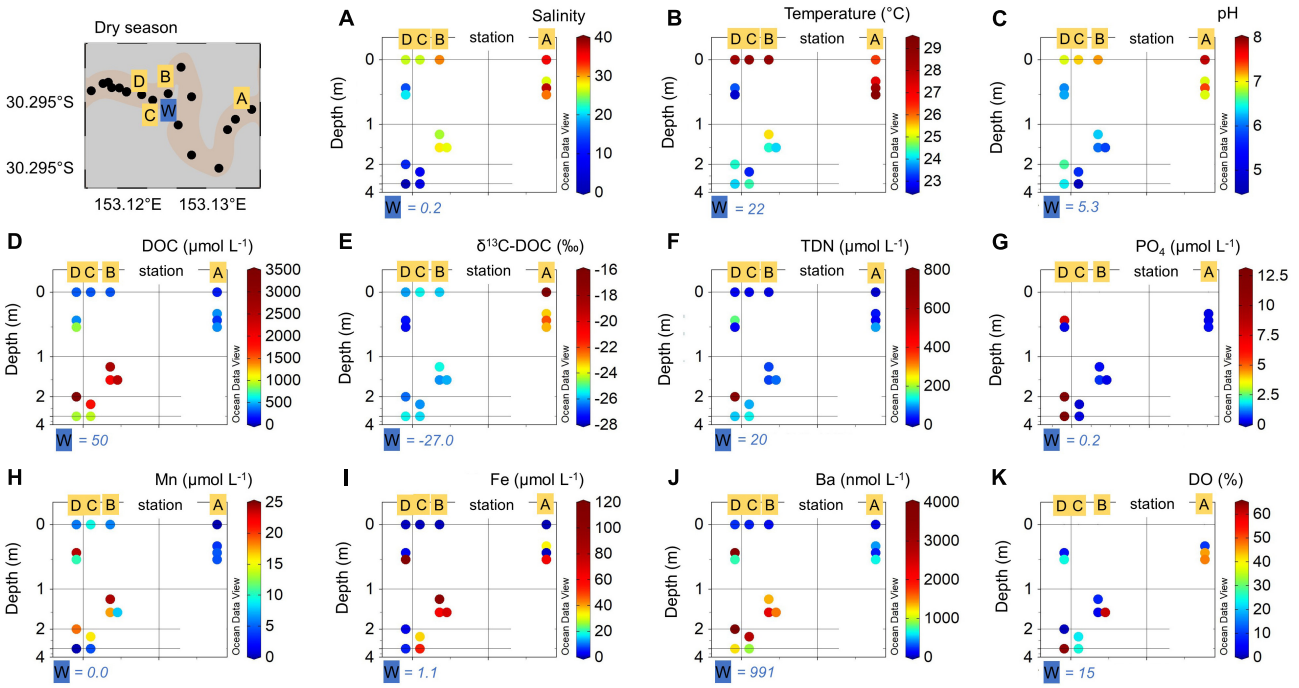

FIGURE 5 | Porewater (A–D) and deep groundwater (*W*) observations during dry season with **(A)** salinity, **(B)** temperature (°C), **(C)** pH, **(D)** dissolved organic carbon (DOC) (µmol L^{-1}), **(E)** δ^{13}C-DOC (‰), **(F)** total dissolved nitrogen (TDN) (µmol L^{-1}), **(G)** phosphate (PO_4) (µmol L^{-1}), **(H)** dissolved manganese (Mn) (µmol L^{-1}), **(I)** dissolved iron (Fe) (µmol L^{-1}), **(J)** dissolved barium (Ba) (nmol L^{-1}), and **(K)** dissolved oxygen saturation (DO) (%), at the porewater stations A–D (yellow squares) in different depths (A–D = 0.3–4 m) and in the deep fresh groundwater endmember (*W* = 28 m; blue square) along the salinity transect compared to surface water concentrations (depth = 0 m). The *y*-axis represents the depth (m) relative to the sediment surface. The *x*-axis represents the location of the respective porewater sampling site (latitude in degrees east) along the estuarine gradient, as shown in the map in top left corner.

TABLE 1 | Characteristics DOM molecular formulae (intensity-weighted averages ± intensity-weighted standard deviation) of the molecular endmembers (marine, mangrove and fluvial) as identified by principal coordinate analyses.

	Dry season			Wet season		
	Marine[2]	**Mangrove**	**Fluvial**	**Marine**	**Mangrove**	**Fluvial**
Formulae[1]	100	274	30	324	239	267
Mass (Da)	601 ± 221	552 ± 179	438 ± 156	528 ± 80	566 ± 194	539 ± 186
C	30.0 ± 13.2	27.0 ± 11.2	22.2 ± 8.3	23.0 ± 4.7	28.2 ± 11.7	26.3 ± 10.0
H	34.1 ± 22.1	35.0 ± 18.4	21.6 ± 12.8	28.3 ± 7.3	31.4 ± 18.7	28.3 ± 17.0
O	10.7 ± 7.1	10.3 ± 5.5	7.4 ± 4.9	11.7 ± 3.4	10.4 ± 5.8	10.1 ± 5.9
N	1.11 ± 1.35	0.89 ± 1.25	0.95 ± 1.00	0.91 ± 1.12	1.07 ± 1.32	1.00 ± 1.29
S	0.39 ± 0.58	0.27 ± 0.56	0.36 ± 0.64	0.41 ± 0.49	0.37 ± 0.57	0.45 ± 0.66
P	0.31 ± 0.46	0.26 ± 0.44	0.23 ± 0.43	0.39 ± 0.49	0.15 ± 0.36	0.16 ± 0.37
H/C	1.17 ± 0.50	1.31 ± 0.47	0.94 ± 0.37	1.25 ± 0.30	1.11 ± 0.44	1.06 ± 0.43
O/C	0.40 ± 0.26	0.43 ± 0.23	0.34 ± 0.24	0.53 ± 0.17	0.41 ± 0.23	0.41 ± 0.22
AI_{mod}[3]	0.33 ± 0.28	0.25 ± 0.29	0.48 ± 0.28	0.19 ± 0.20	0.35 ± 0.27	0.39 ± 0.26
DBE[4]	14.60 ± 10.61	11.06 ± 8.53	13.06 ± 5.70	10.53 ± 4.18	14.10 ± 8.55	13.75 ± 7.43

[1]Exclusive molecular formulae; [2]Marine endmember ($S1_{dry}$; $S1_{wet}$), mangrove endmember ($S10_{dry}$; $S10_{wet}$), fluvial endmember ($S18_{dry}$; $S18_{wet}$); [3]Aromaticity index (AI_{mod}) as described by Koch and Dittmar (2006, 2016); [4]Double bond equivalents (DBE).

(2) mangrove, and (3) fluvial. During the dry season, we identified a fourth cluster consisting of station 7 and 17 (**Supplementary Figure S2**).

To investigate the processes related to changes in the molecular DOM composition along the estuarine gradient, we correlated the environmental parameters to the DOM molecular composition in PCoA (**Figure 6**). During dry season, principal coordinate 1 (PC1), which explained 81% of the variability of the DOM molecular composition, was related to TDN and Ba concentrations, salinity as well as the relative abundance

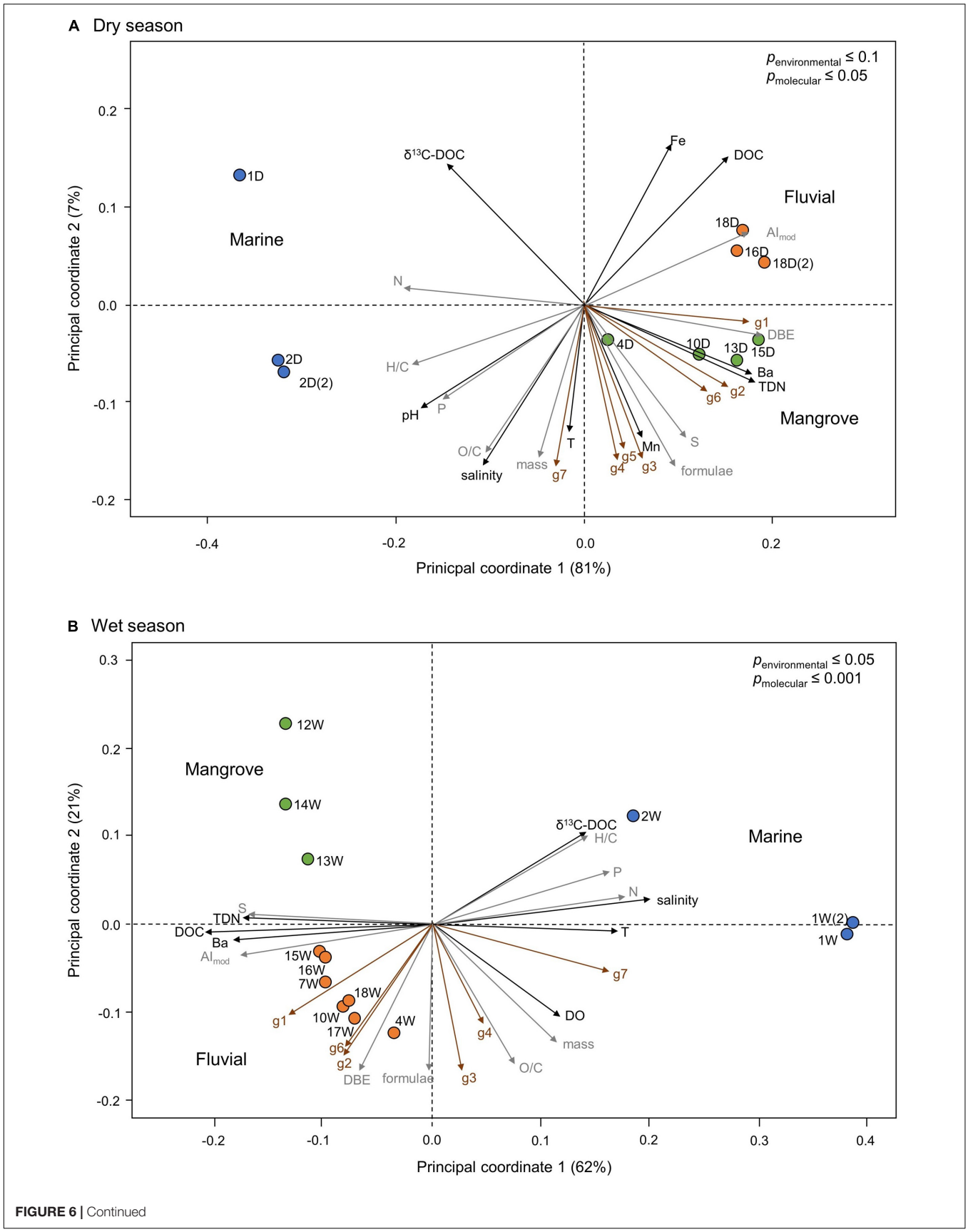

FIGURE 6 | Continued

FIGURE 6 | Principal coordinate analyses (PCoA) based on Bray–Curtis dissimilarity of the relative FT-ICR-MS signal intensities of DOM molecular formulae. Panel **(A)** the dry and panel **(B)** the wet season. The percentages depict the DOM molecular variability as explained by the respective axes. Colored circles represent the identified main DOM clusters: marine (blue circles), mangrove (green circles) and fluvial (orange circles). The environmental parameters (black arrows for Fe, DOC, Ba, TDN, Mn, salinity, pH, DO, T, and δ^{13}C-DOC) were significantly correlated with $p \leq 0.1$ and 0.05 in the dry and wet season, respectively. Intensity-weighted averages of DOM molecular parameters (gray arrows for H/C, O/C, N, P, S, DBE, AI_{mod}, number of molecular formulae and masses) and DOM molecular compound groups (red arrows) were significantly correlated with $p \leq 0.05$ or 0.001 in the dry and wet season, respectively. DOM molecular compound groups were defined after Seidel et al. (2017); i.e., g1: polycyclic aromatic, g2: highly aromatic, g3: highly unsaturated, g4: unsaturated aliphatic, g5: saturated compounds with low O/C ratios, g6: saturated compounds with high O/C ratios, and g7: aliphatic compounds containing N. Correlations of Fe, Mn, and g5 during the wet season were not significant and therefore are not shown.

of molecular compound groups g1, g2, and g6, separating the marine from the mangrove and fluvial cluster. The mangrove and fluvial cluster were separated by PC2 (7%), which was related to DOC and Fe concentrations (**Figure 6A**). During the wet season, PC1 explained 62% of the DOM molecular variability, separating the marine from the mangrove and fluvial clusters. PC1 was related to TDN, DOC, Ba concentrations as well as the relative abundance of organic sulfur compounds and aromaticity (AI_{mod}) (**Figure 6B**). The mangrove and fluvial clusters were separated by PC2, which explained 21% of the DOM molecular variability in the wet season.

During both seasons, samples clustering in the marine group were related to higher δ^{13}C-DOC values, higher H/C ratios as well as higher intensity weighted averages of molecular phosphorous (P_{mol}) and N_{mol}. During the wet season, samples from the marine cluster were additionally related to salinity, water temperature and the molecular compound group g7. During the dry season, the samples from the fluvial cluster were related to Fe and DOC concentrations as well as aromaticity (AI_{mod}). During the wet season, the samples from the fluvial cluster were additionally related to the weighted-average double bond equivalents (DBE), TDN concentration, Ba concentration, intensity weighted-averages of molecular sulfur (S_{mol}) as well as the relative abundances of DOM compound groups g1, g2, and g6. The mangrove cluster during the dry season was related to the Ba, TDN, and Mn concentrations as well as weighted-averages of S_{mol}, DBE, and DOM compound groups 1–6.

As major compound classes of the DOM pool have characteristic molar ratios of H/C and O/C, we correlated the PCoA object scores of the main axes to the original DOM molecular formulae to assess their contribution to the ordination (Ramette, 2007). These correlations can be displayed in Van Krevelen Diagrams (van Krevelen, 1950). Certain chemical classes cluster in specific areas (Kim et al., 2003; Minor et al., 2014), which allows to identify processes and environmental drivers represented by the different principal coordinates (**Figure 7**). During both seasons, PC1 was mainly related to the mixing between terrestrial and marine DOM. We observed the general pattern of high O/C ratios in the fluvial and mangrove cluster shifting toward lower ratios in the marine cluster. H/C ratios showed the opposite trend with generally higher values in the marine cluster and lower values in the mangrove and fluvial cluster. The loading of PC2 during the wet season was mainly related to high O/C ratios in the fluvial cluster and a shift toward lower ratios in the mangrove and marine cluster.

DISCUSSION

Sources and Sinks in the Estuary: Mixing and Porewater-Exchange

The mixing analysis of the bulk parameters demonstrates complex processing of the DOM and inorganic chemical species along the estuarine gradient (summarized in conceptual model in **Figure 8**). The concentrations of organic and inorganic bulk parameters were above (Mn, Ba, DOC, and TDN) or below (Fe and δ^{13}C-DOC) values expected from conservative mixing of fluvial and marine endmembers, indicating removal and addition of these chemical species, respectively (**Figure 4**).

The cycling of Mn and Fe is closely linked to the prevailing redox conditions. These trace metals can be transferred between the dissolved and particulate phase through reduction (dissolution) and oxidation (precipitation) of Mn-/Fe-oxyhydroxides (Sholkovitz, 1978; Chester and Jickells, 2012). While we observed an input of dissolved Mn along the estuarine gradient, the decrease of dissolved Fe concentrations indicates that the estuary acts as a sink for dissolved Fe during both seasons. The deviation from values expected from conservative mixing was most prominent in the lower fluvial-mangrove transition zone and upper mangrove-fringed zone of the estuary (**Figure 4** and **Table 2**). In intertidal systems, Fe can be released through Fe(hydr)oxide dissolution under suboxic to anoxic conditions. Dissolved Fe can be removed due to precipitation as iron monosulfides (FeS) under sulfidic conditions or Fe(hydr)oxides in oxygen-rich environments (Beck et al., 2008). Mn is mostly associated with Mn(hydr)oxide dissolution during suboxic to anoxic conditions and precipitation of dissolved Mn during oxic conditions (Burdige, 1993; Beck et al., 2008). Especially in organic-rich environments, the mobility of Fe and Mn is often enhanced by organo-metallic complexes (Chapman et al., 1998).

The wetland and mangrove porewaters in our system were hypoxic with high concentrations of DOC, dissolved Mn and Fe (**Figure 5**). The high concentrations of the redox-sensitive trace metals Mn and Fe can be explained by Mn- and Fe-reducing (benthic) microbes which utilize Fe- and Mn(hydr)oxides as terminal electron acceptors in the sediments to oxidize organic matter when molecular oxygen is exhausted (Luther et al., 1992; Burdige, 1993; Beck et al., 2008; Reddy and DeLaune, 2008). Sulfidic soils are common for coastal wetlands and mangrove systems of Australia (Fitzpatrick et al., 2008). We observed a distinct hydrogen sulfide smell as well as high concentrations of DOC and low oxygen saturation in the porewater compared to the surface waters (**Figure 5**) indicating active microbial

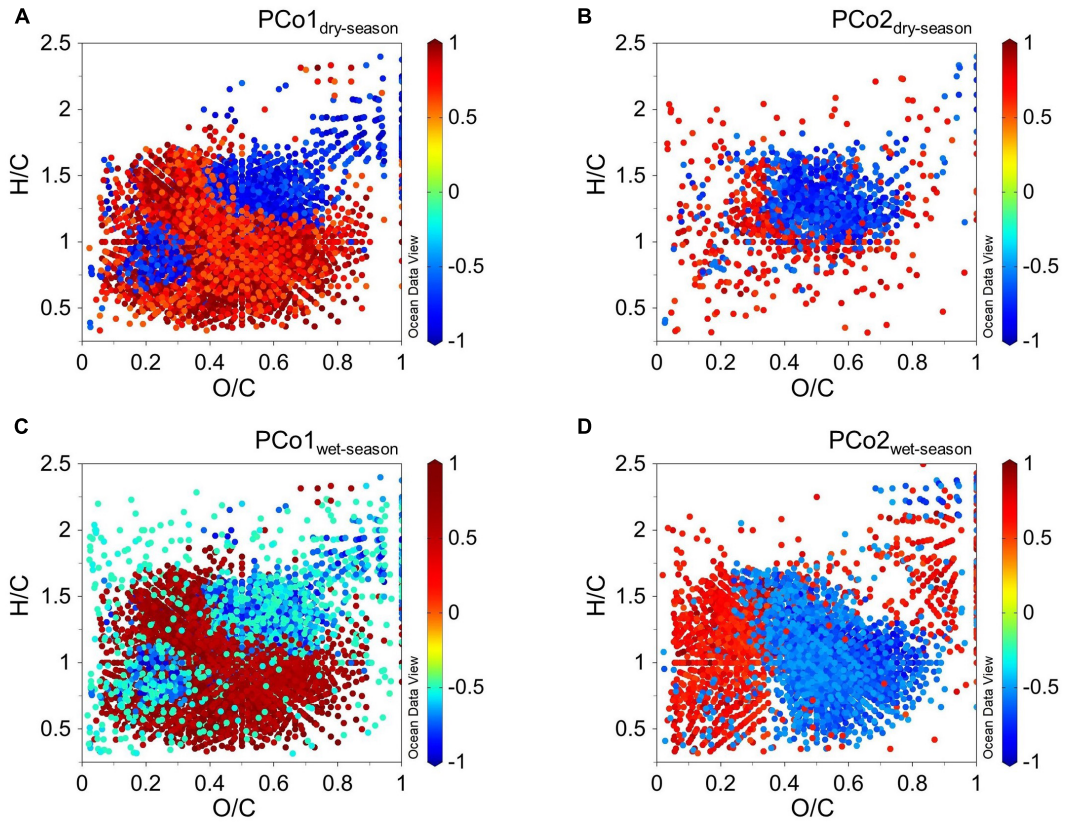

FIGURE 7 | Van Krevelen plots showing the color-coded correlations of molecular formulae with the scores of principal coordinate analysis **(A)** PCo1 in dry season, **(B)** PCo2 in dry season, **(C)** PCo1 in wet season, and **(D)** PCo2 in wet season.

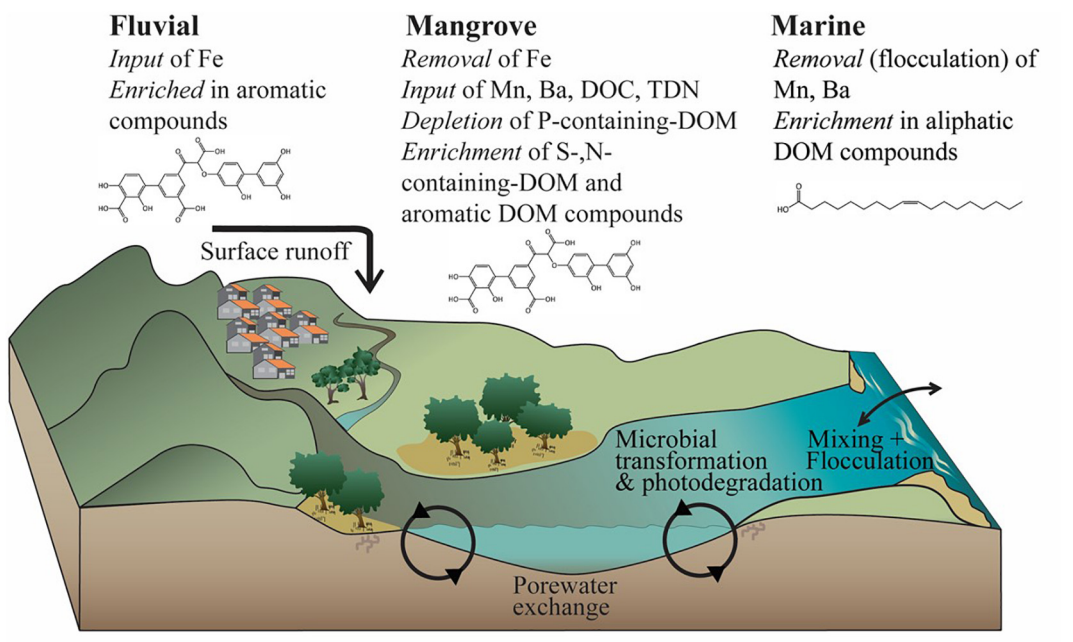

FIGURE 8 | Conceptual model summarizing the key processes influencing organic and inorganic matter cycling along the estuarine transect in Coffs Creek Estuary.

TABLE 2 | Deviations of the concentrations of organic and inorganic surface water constituents from conservative mixing values during dry season in different zones along the estuarine gradient as calculated by box models.

Box	Zone	Corresponding time series station	Net-flux ($m^3\ s^{-1}$)[1]	ΔDOC ($\mu mol\ L^{-1}$)	$\Delta\delta^{13}$C-DOC (‰)	ΔTDN ($\mu mol\ L^{-1}$)	ΔMn ($\mu mol\ L^{-1}$)	ΔFe ($\mu mol\ L^{-1}$)	ΔBa ($nmol\ L^{-1}$)
1	Marine	A	0.9	11	1.0	0	0.0	−0.05	44
2	Mangrove-fringed	B/C	0.3/0.008	137	−1.0	6	5.0	−0.07	60
3	Fluvial-mangrove transition	D	0.05	98	−0.3	13	7.0	−0.34	119
4	Fluvial	E	0.01	10	0.2	5	4.5	−0.08	84

[1]*Net-discharge measurements over a complete tidal cycle (25 h) at the corresponding time series stations/porewater sites (**Figure 1**).*

sulfate reduction in the adjacent creek sediments. In urban areas, untreated wastewater may be a source of reduced sulfur species to the surface waters. However, Reading et al. (2017) found that sewage is not an important source of reduced chemical species to the tidal creek and there is no significant discharge of untreated sewage or wastewater to Coffs Creek Estuary (GeoLINK, 2013). Therefore, we assume that the input of reduced sulfur species is mainly related to tidally driven porewater exchange from the sulfidic mangrove sediment and tidal flushing of mangrove crab burrows (Sadat-Noori et al., 2017). The removal of dissolved Fe from the surface waters is therefore likely related to (1) the formation of insoluble Fe-sulfides in the adjacent mangrove sediments, and (2) to the co-precipitation and flocculation due to changes in ionic strength in the estuarine turbidity maximum zone (Sholkovitz, 1978), which is located in the upper fluvial and fluvial-mangrove transition zones (GeoLINK, 2013). The high concentrations of Mn in mangrove porewaters (**Figure 5**) suggest porewater discharge as an important source of dissolved Mn to the surface creek waters, which was previously observed in other mangrove-fringed estuaries as well (Holloway et al., 2016). Since Fe and Mn are essential micronutrients (Sunda, 1989, 2000), active biological removal (e.g., by phytoplankton) is likely an additional sink in the estuary.

Several studies on Ba cycling in coastal ocean areas and land ocean transition zones have reported non-conservative behavior of Ba in estuaries due to processes such as solute-particle interactions. Thus, its application in these systems ranges from being used as a tracer for mixing (Moore, 1997; Gonneea et al., 2008) to a tracer for marine primary production (Stecher and Kogut, 1999). Ba cycling in estuaries is largely driven by ion exchange processes on particles in response to changes in ionic strength and Ba shows a strong affinity to Mn (Shaw et al., 1998; Charette et al., 2005; Charette and Sholkovitz, 2006; Santos et al., 2011a). Fluvial-derived suspended particles are often considered to be a major source for Ba to surface estuaries (e.g., Moore and Shaw, 2008; Samanta and Dalai, 2016). Increasing salinity along the estuarine transect drives Ba desorption from the riverine particles, which often results in a mid-salinity increase of Ba along estuarine gradients (e.g., Hanor and Chan, 1977; Coffey et al., 1997). Additionally, Ba can be added to porewater during the dissolution of Fe and Mn(hydr)oxides in sediments under suboxic to anoxic conditions (Gonneea et al., 2008; Singh et al., 2013). Thus, comparable to radium, Ba is mobilized and released to surface waters through porewater discharge (Peterson et al., 2008). We found positive deviations of Ba concentrations from values expected from conservative mixing in the mid-section of the estuary (**Figure 4** and **Table 2**). This input of Ba appears to be driven by two major processes: (1) the dissolution of Ba from riverine particles in the fluvial-mangrove transition zone (low to mid-salinity increase (Coffey et al., 1997) and (2) the coupled release of Ba and Mn from the anoxic sediments and porewaters and their discharge into the surface creek waters (mangrove-fringed zone). Even though we observed a high input of dissolved Mn and Ba along the estuarine basin, most of the derived solutes were removed before reaching the coastal ocean (**Figures 2**, **3**). This removal in the lower section was most likely induced by increasing pH values (**Figure 2**), and a higher oxygen saturation in the water column compared to the porewater (Sadat-Noori et al., 2017), which leads to the oxidation and precipitation of Mn and a co-precipitation of Ba (Coffey et al., 1997). Ba as well as Mn have been shown to be involved in (marine) primary production processes (Bishop, 1988; Sunda, 1989, 2000; Stecher and Kogut, 1999). Thus, removal of Ba due to the formation of biogenic barite (e.g., opal by diatoms) may be a possible Ba sink (Bruland, 1983; Bishop, 1988).

Nitrogen cycling in estuaries is driven by a complex interaction of oxygen availability, organic matter supply, groundwater inputs, microbial activity and mixing of different water masses (Wong et al., 2013; Murray et al., 2015). In the fluvial-mangrove transition and mangrove-fringed zone TDN concentrations increased strongly (**Figures 2**, **3**). Reading et al. (2017) showed a shift from nitrate in the fluvial endmember to ammonium and DON toward the marine endmember of the Coffs Creek Estuary. The increase of TDN concentrations suggest that the oxygen-depleted mangrove porewaters are an important source for TDN such as ammonium and DON to the creek surface waters, particularly in the mangrove-fringed zones where tidally driven porewater exchange takes place.

All DOC concentrations during the dry season were above values expected from conservative mixing indicating a source of DOC (**Figure 4**). This DOC source was most pronounced in the lower fluvial-mangrove transition and mangrove-fringed zone. Scatter plots for δ^{13}C-DOC indicated ^{13}C-depleted DOC (δ^{13}C-DOC values −24.2 to −25.5‰) in the mangrove-fringed section (**Figure 4**). Since we also observed an enrichment of DOC in the mangrove porewaters, we suggest mangrove-derived input of DOC in this area. Interestingly, we observed a strong decrease of dissolved Mn, Fe, and DOC concentrations in the marine zone of the estuary (area with salinity > 30; **Figure 4**). The δ^{13}C-DOC values in the marine zone were also more ^{13}C enriched,

indicating an input of ^{13}C enriched (marine planktonic) DOC and/or removal of ^{13}C depleted terrestrial DOC. Altogether, these trends suggest removal of terrestrial DOC through co-precipitation and adsorption on Fe and Mn particles and an input of marine (planktonic) DOC in the less turbid part of the estuary (**Figure 8**).

Drivers of Molecular Transformations of DOM

The molecular DOM composition can undergo estuarine transformations due to input and removal processes. These molecular changes are not necessarily reflected by changes in the bulk DOC concentrations. Thus, we related the estuarine DOM molecular composition to the measured bulk parameters to determine the environmental drivers of it (**Figures 4**, **6**). Both, molecular DOM compounds and bulk parameters along the estuarine gradient showed a considerable deviation from simple mixing of the fluvial and marine endmembers indicating transformation of DOM along the transect.

We identified the molecular DOM composition of the three main clusters with their respective: (1) marine, (2) terrestrial, and (3) mangrove endmembers (**Figure 6**). The definition of endmembers based on salinity was found to be not suitable to distinguish between the mangrove (high salinity, anoxic porewater with terrestrial organic matter input) and marine (high salinity, oxic with marine organic matter input) endmembers. Thus, in our study we defined the endmembers based on the DOM molecular composition in addition to the environmental parameters salinity, sampling location, redox condition, DOC concentration, and $\delta^{13}C$-DOC values. The terrestrial and mangrove endmembers were enriched in aromatic compounds (compound groups g1 and g2, characterized by AI_{mod} values >0.5) compared to the marine DOM endmember. We found scattered input of unsaturated aliphatic (compound group g4, **Figure 4**) and saturated compounds (compound group g5, **Supplementary Figure S1**) in the mangrove-fringed zone of the estuary. The saturation of the DOM compounds increased from the fluvial to the marine endmember samples (higher weighted-average H/C ratios and lower weighted-average AI_{mod} values in **Table 1**). This is because marine DOM is enriched in aliphatic structures, while river water has a higher content of terrestrial aromatic compounds such as polyphenols (Medeiros et al., 2015; Seidel et al., 2015; Osterholz et al., 2016). We found a high input of aromatic DOM compounds in the mangrove-porewater dominated area (e.g., compound groups 1 and 2, **Figure 4** and **Supplementary Figure S1**), which was particularly pronounced during the dry season. Remarkably, this more aromatic DOM signal appeared not to be transported to the coastal marine zone. This can be explained with the mixing of the aromatic terrestrial DOM with the more aliphatic marine DOM compounds in the high salinity (>30) marine zone. Additional processes that can account for the removal of aromatic DOM compounds in estuaries leading to a more aliphatic DOM signature are photodegradation in the less turbid parts of the estuarine mixing (Dittmar et al., 2006; Gonsior et al., 2009; Medeiros et al., 2015; Osterholz et al., 2016) and co-precipitation during the flocculation of Mn or Fe solid phases (Sholkovitz, 1978; Moore et al., 1979) (**Figure 8**).

The stations in the mangrove-fringed and fluvial-mangrove transition zones received an input of highly aromatic, unsaturated aliphatic and saturated DOM compounds as well of S-containing DOM (**Figure 4**). These DOM compounds are indicative for biotransformation of terrestrial DOM and input of autochthonous microbial DOM (Kujawinski et al., 2004; Sleighter and Hatcher, 2008; Medeiros et al., 2015; Osterholz et al., 2016) as well as porewater-exchange-driven input of sulfur-containing DOM from sulfidic porewaters (Schmidt et al., 2009; Seidel et al., 2014; Sleighter et al., 2014). Sulfur-enriched DOM is generally observed in sulfidic enviroments and can be the result of abiotic chemical reactions of sulfide with DOM (Schmidt et al., 2009; Gomez-Saez et al., 2016; Pohlabeln et al., 2017). As the respective DOM molecular formulae from the mangrove cluster were also related to the higher dissolved Ba, Mn, and TDN concentrations (**Figure 6**), we suggest that the mangrove-fringed zone is strongly influenced by the input of microbially transformed mangrove DOM from the mangrove porewaters.

The DOM molecular formulae of the marine endmember were characterized by higher relative weighted-averages of N- and P-atoms as well as higher weighted-average H/C ratios compared to the terrestrial and mangrove endmembers (**Table 1**). Besides the mixing of estuarine waters with the marine endmember, these enrichments of N- and P heteroatoms and aliphatic compounds can be explained by the input of marine DOM from phytoplankton and microbial production as well the as transformation of terrestrial DOM (Gonsior et al., 2011; Medeiros et al., 2015; Osterholz et al., 2016).

The Influence of Rain Events on Fluxes to the Coastal Ocean

Large flood-events can release a pulse of terrigenous DOM from river catchments, a process that has been termed "pulse-shunt-concept" (Raymond et al., 2016). This DOM pulse may be rapidly transported along the river toward the coastal ocean, while being relatively unaffected by the estuarine filter. The catchment area of Coffs Creek Estuary is largely deforested and subject to urban and agricultural pressure, which leads to increasing runoff during heavy rain events (GeoLINK, 2013). We hypothesized that a heavy rain event leads to the enhanced input of DOM and inorganic constituents across the estuary into the coastal ocean.

During the wet season, the values of bulk DOC concentrations and the DOC-normalized relative abundances of the molecular DOM parameters along the estuarine gradient followed a conservative mixing trend. This indicates less biogeochemical transformations in the estuary under wet conditions compared to dry conditions (**Figure 4** and **Supplementary Figure S1**). In line with the pulse-shunt concept it also shows that the influence of tidally driven porewater exchange was smaller during the rainy season, probably due to the increased flow conditions, shorter residence time and less exchange with the mangrove sediments. We suggest that the mixing of the fluvial and marine endmembers was the dominant process responsible for the DOM distribution during the wet season in Coffs Creek Estuary (**Figure 4** and

Supplementary Figure S1). However, the δ^{13}C-DOC and DOM molecular components mixing models (**Figure 4**) as well as statistical analysis (**Figure 6**) showed additional alterations of the DOM isotopic and molecular composition. For example, the surface water DOC was more ^{13}C enriched in the fresh headwaters of the estuary compared to dry season. Yet this signal was strongly shifted to more ^{13}C depleted DOC in the mangrove-dominated area (**Figure 4**). These δ^{13}C-DOC values are in the range of previously reported ^{13}C depleted DOC values from mangrove sources in the mangrove-fringed zone (Maher et al., 2013). In the same area we observed the input of aromatic and S-containing molecular DOM components, which indicates an input of highly aromatic DOM compounds (e.g., polyphenols) and sulfur-enriched DOM from the adjacent sulfidic mangrove porewaters and catchment area. Terrestrial organic matter such as degraded lignin and tannin have been previously described as important DOM sources in a mangrove-fringed estuary (Dittmar et al., 2001, 2006). Our data demonstrate that the estuarine surface waters were relatively enriched with DOM compounds from the surrounding mangroves, even under high-discharge conditions, although this molecular fingerprint was less pronounced compared to dry conditions.

In line with the "pulse-shunt concept" described above, Sanders et al. (2015) hypothesized that due to the high organic matter load and shorter residence times the estuarine filter might be inhibited in small tidal creeks compared to bigger estuarine systems. We calculated the effective export flux of DOC as well as dissolved Mn, Fe, Ba, and TDN from river to estuary and from the estuary to the coastal ocean using the standard estuarine model (Kaul and Froelich, 1984) for the dry and wet season (**Table 3**). The average freshwater discharge in Coffs Creek Estuary in 2016 was 10^7 m^3 year^{-1} (BOM, 2016). Based on the catchment area (24.5 km^2) and endmembers defined by salinity and location we calculated an average annual flux (mean of dry and wet surveys) for dissolved Fe (1,988 mol km^{-2} year^{-1}), Mn (237 mol km^{-2} year^{-1}), and Ba (48 mol km^{-2} year^{-1}) as well as DOC (174,465 mol km^{-2} year^{-1}) and TDN (16,647 mol km^{-2} year^{-1}) (**Table 3**).

We also calculated the effective export flux from the estuary to the ocean, where C_{fw} is the measured concentration in the freshwater and C^*_{fw} is the calculated concentration in the estuarine mixing zone after production or removal have taken place (**Table 3**). If C^*_{fw} of a chemical species is lower (or higher) than the measured concentrations in the freshwater (C_{fw}), than the estuary is a sink (or source) for this chemical species (Santos et al., 2009). In our case, the effective freshwater concentrations were higher (Mn, Ba, DOC, TDN) or lower (Fe) than the riverine concentrations, confirming the presence of sources (for Mn, Ba, DOC, TDN) and sinks (for Fe) along the estuarine transect, respectively. The annual flux as well as the effective export flux calculations based on only dry and wet conditions considerably differ from each other. This implies that the strength of the estuarine filter as well as mangrove sources and sinks were also highly variable and depended strongly on the present flow conditions and residence times. These calculations demonstrate that intertidal mangroves can govern

TABLE 3 | Dissolved inorganic solutes (Mn, Fe, and Ba), TDN and DOC river fluxes (C_{fw}) as well as effective export fluxes (C^*_{fw}) at Coffs Creek Estuary during dry and wet conditions.

	Dry conditions		Wet conditions		Average	
	C_{fw}	C^*_{fw}[1]	C_{fw}	C^*_{fw}	C_{fw}	C^*_{fw}
Concentration[2]						
Fe (nmol L^{-1})	2,100	1,299	4,787	2,772	3,444	2,036
Mn (nmol L^{-1})	30	37,003	579	4,327	305	20,665
Ba (nmol L^{-1})	162	594	112	161	137	378
DOC (μmol L^{-1})	336	1,339	414	463	375	901
TDN (μmol L^{-1})	20	46	40	73	30	59
Fluxes (mol year^{-1})[3]						
Fe	1,680	1,039	95,740	55,440	48,710	28,240
Mn	24	29,602	11,580	86,540	5,802	58,071
Ba	130	475	2,240	3,220	1,184	1,848
DOC	268,800	1,070,960	8,280,000	9,260,000	4,274,400	5,165,480
TDN	15,680	36,712	800,000	1,460,000	407,840	748,356
Catchment area fluxes (mol km^{-2} year^{-1})[4]						
Fe	69	42	3,908	2,263	1,988	1,153
Mn	1	1,208	478	3,532	237	2,370
Ba	5	19	91	131	48	75
DOC	10,971	43,713	337,959	377,959	174,465	210,836
TDN	640	1,498	32,653	59,592	16,647	30,545

[1]Effective export flux from the estuary into the ocean calculated based on a standard estuarine model according to Kaul and Froelich (1984) and Santos et al. (2009); [2]Fluvial endmember concentrations; [3]Average annual discharge calculated based on data acquired from BOM (2016). Freshwater discharge was 0.02 and 0.550 m^3 s^{-1} during dry and wet conditions, respectively; [4]Catchment area fluxes were estimated dividing the total fluxes by the catchment area (24.5 km^2).

TABLE 4 | Summary of literature data on dissolved organic carbon (DOC) outwelling in mangrove dominated areas.

Country	Site	Mangrove area (km^2)	DOC outwelling (mmol m^{-2} day^{-1})	Setting	Data Source[1]
Northern Brazil	Caeté River	190	11	Largely pristine (protected mangrove area)	Dittmar and Lara, 2001
	North Brazilian shelf	10,000	33	Largely pristine (protected mangrove area)	Dittmar et al., 2006
Florida, United States	Shark and Harney River	NA[2]	25	Pristine (Everglades National Park)	Ho et al., 2017
	Shark River	NA	13	Pristine (Everglades National Park)	Romigh et al., 2006
	Taylor River	60	87	Pristine (mangrove island enclosures, Everglades National Park)	Davis et al., 2001
	Rookery Bay Estuary	15	11	Adjacent to Everglades National Park	Twilley, 1985
Tanzania	Zanzibar	0.4	53	Urban (partly contaminated with sewage waste)	Machiwa, 1999
India	Sundarbans	4,264	162	Pristine (UNESCO world heritage site)	Ray et al., 2018
Vietnam	Unnamed tidal creek in Can Gio Mangrove Forest	0.5	21–68	Pristine (Can Gio UNESCO biosphere reserve)	Taillardat et al., 2018
Australia	Moreton Bay	37.8	6–25	NA[2]	Maher et al., 2013
	Jacobs Well	0.4	42	NA	Sippo et al., 2017
	Coral Creek	0.1	5	NA	Ayukai et al., 1998
	Coffs Creek Estuary	0.2	13	Urban (agriculture)	This study

[1]*Adapted from Bouillon et al. (2008) and updated with more recent data;* [2]*NA = information not available.*

the efficiency of the estuarine filter. Mangroves are known to be important drivers for the coastal organic and inorganic element budgets. DOC outwelling rates from mangrove forests at different locations around the globe show considerable differences ranging between 5 and 162 mmol m^{-2} day^{-1} (**Table 4**). We normalized the differences between river fluxes (C_{fw}) and effective river flux (C^*_{fw}) to the present mangrove area (187,000 m^2, Sadat-Noori et al., 2017) to estimate the influence of mangroves on organic and inorganic matter cycling in Coffs Creek Estuary. The estimated DOC drainage from mangrove forests in Coffs Creek estuary amounts to 13 mmol m^{-2} day^{-1} which is within the lower range of the findings elsewhere (**Table 4**). Our calculations further reveal that tidally driven porewater exchange in mangrove sediments lead to an annual increase of dissolved Mn, Ba as well as DOC and TDN and a decrease of dissolved Fe concentration by a factor of 10, 1.6, 1.2, 1.8, and −0.4, respectively.

CONCLUSION

We combined bulk geochemical parameter analysis with non-targeted molecular DOM analysis to reveal biogeochemical transformations along a mangrove-fringed estuary. Tidally driven porewater exchange with sediments in the adjacent mangrove forests led to a removal of dissolved Fe (depleted concentration by a factor of −0.4) and an enrichment of dissolved Mn (by factor 10), Ba and TDN (by factor 1.6) as well as DOC (by factor 1.2). After passage through the mangrove-fringed zone, phosphorous containing DOM compounds were relatively depleted in the creek surface waters. In contrast, sulfur- and nitrogen-containing DOM as well as aromatic DOM compounds were relatively enriched in the surface creek waters, which we ascribe to the discharge of mangrove porewater. In the high salinity zone of the estuary, additional autochthonous (microbial) sources and the removal of aromatic DOM compounds, probably due to photodegradation and co-precipitation along with metals such as Mn caused a shift to a more aliphatic DOM signature toward the marine zone (see conceptual model in **Figure 8**). The observed biogeochemical transformations were less pronounced during wet compared to dry conditions, which we ascribe to shorter residence times and hence less exchange with the mangrove sediments. Our flux calculations showed that mangroves affect estuarine biogeochemical processes and may be important sources of DOM and inorganic nutrients (TDN, Mn) to the ocean. Our study confirms that mangroves have a fundamental impact on the DOM, nutrient and trace metal cycling in estuaries. In comparison to other estuarine systems, biogeochemical processes in mangrove-fringed estuaries may have an even more important function in buffering nutrients, trace metal and DOM fluxes to the coastal ocean between high and low discharge events, than previously assumed.

DATA AVAILABILITY

Data used to produce the results of this manuscript can be obtained by contacting CM.

AUTHOR CONTRIBUTIONS

CM, IS, and MS conceived the study. CM performed the chemical analyses. IS provided the dissolved carbon, nitrogen, and phosphorous data. BS, TD, and H-JB contributed to the chemical analysis and the data interpretation. CM wrote the manuscript with significant contributions from all authors.

FUNDING

This work was supported by the Australian Research Council (FT170100327 and LE170100007).

ACKNOWLEDGMENTS

We thank Ceylena Holloway, Michael Reading, Luke Jeffrey, Arun Looman, Summer Barrow, Damien Maher, and Douglas Tait (National Marine Science Centre, Southern Cross University) for their valuable help during sampling. Eleonore Gruendken and Katrin Klaproth (ICBM, University of Oldenburg) were thanked for their excellent technical assistance during trace metal and molecular dissolved organic matter analyses, respectively. This study was carried out in the framework of the Ph.D. research training group "The Ecology of Molecules" (EcoMol) supported by the Lower Saxony Ministry for Science and Culture. We acknowledge the two reviewers and the editor for their thoughtful and valuable comments, which led to an improved manuscript.

SUPPLEMENTARY MATERIAL

The Supplementary Material for this article can be found online at: https://www.frontiersin.org/articles/10.3389/fmars.2019.00481/full#supplementary-material

REFERENCES

Alongi, D., Sasekumar, A., Tirendi, F., and Dixon, P. (1998). The influence of stand age on benthic decomposition and recycling of organic matter in managed mangrove forests of Malaysia. *J. Exp. Mar. Biol. Ecol.* 225, 197–218. doi: 10.1016/s0022-0981(97)00223-2

Ayukai, T., Miller, D., Wolanski, E., and Spagnol, S. (1998). Fluxes of nutrients and dissolved and particulate organic carbon in two mangrove creeks in northeastern Australia. *Mangroves and Salt Marshes* 2, 223–230.

Bauer, J., and Bianchi, T. (2011). Dissolved organic carbon cycling and transformation. treatise on estuarine and coastal science. *Acad. Press, Waltham* 5, 7–67. doi: 10.1016/B978-0-12-374711-2.00502-7

Beck, M., Dellwig, O., Schnetger, B., and Brumsack, H.-J. (2008). Cycling of trace metals (Mn, Fe, Mo, U, V, Cr) in deep pore waters of intertidal flat sediments. *Geochim. Cosmochim. Acta* 72, 2822–2840. doi: 10.1016/j.gca.2008.04.013

Bhatia, M. P., Das, S. B., Longnecker, K., Charette, M. A., and Kujawinski, E. B. (2010). Molecular characterization of dissolved organic matter associated with the Greenland ice sheet. *Geochim. Cosmochim. Acta* 74, 3768–3784. doi: 10.1016/j.gca.2010.03.035

Bishop, J. K. (1988). The barite-opal-organic carbon association in oceanic particulate matter. *Nature* 332, 341–343.

BOM (2016). *Australian Landscape Water Balance*. Available at: http://www.bom.gov.au/water/landscape/ (accessed January 1, 2019).

Bouillon, S., Borges, A. V., Castañeda-Moya, E., Diele, K., Dittmar, T., Duke, N. C., et al. (2008). Mangrove production and carbon sinks: a revision of global budget estimates. *Global Biogeochem. Cycles* 22: GB2013.

Bouillon, S., Frankignoulle, M., Dehairs, F., Velimirov, B., Eiler, A., Abril, G., et al. (2003). Inorganic and organic carbon biogeochemistry in the gautami godavari estuary (Andhra Pradesh, India) during pre-monsoon: the local impact of extensive mangrove forests. *Global Biogeochem. Cycles* 17: 1114. doi: 10.1029/2002GB002026

Bruland, K. W., and Lohan, M. C. (2003). "6.02 – controls of trace metals in Seawater," in *Treatise on Geochemistry* (Oxford: Pergamon), 23–47.

Bruland, K. W. (1983). "CHAPTER 45 - Trace Elements in Sea-water," in *Chemical Oceanography*, eds J. P. Riley and R. Chester Cambridge, MA: Academic Press, 157–220.

Burdige, D. J. (1993). The biogeochemistry of manganese and iron reduction in marine sediments. *Earth Sci. Rev.* 35, 249–284. doi: 10.1016/0012-8252(93)90040-e

Canfield, D. E. (1989). Reactive iron in marine sediments. *Geochim. Cosmochim. Acta* 53, 619–632. doi: 10.1016/0016-7037(89)90005-7

Chapman, P. M., Wang, F., Janssen, C., Persoone, G., and Allen, H. E. (1998). Ecotoxicology of metals in aquatic sediments: binding and release, bioavailability, risk assessment, and remediation. *Can. J. Fish. Aquatic Sci.* 55, 2221–2243. doi: 10.1139/f98-145

Charette, M. A., and Sholkovitz, E. R. (2006). Trace element cycling in a subterranean estuary: Part 2. geochemistry of the pore water. *Geochim. Cosmochim. Acta* 70, 811–826. doi: 10.1016/j.gca.2005.10.019

Charette, M. A., Sholkovitz, E. R., and Hansel, C. M. (2005). Trace element cycling in a subterranean estuary: part 1. geochemistry of the permeable sediments. *Geochim. Cosmochim. Acta* 69, 2095–2109. doi: 10.1016/j.gca.2004.10.024

Chester, R., and Jickells, T. (2012). *Marine Geochemistry*. Hoboken: John Wiley & Sons.

Coffey, M., Dehairs, F., Collette, O., Luther, G., Church, T., and Jickells, T. (1997). The behaviour of dissolved barium in estuaries. *Estuar. Coast. Shelf Sci.* 45, 113–121. doi: 10.1006/ecss.1996.0157

Davis, S. E., Childers, D. L., Day, J. W., Rudnick, D. T., and Sklar, F. H. (2001). Wetland-water column exchanges of carbon, nitrogen, and phosphorus in a southern Everglades dwarf mangrove. *Estuaries* 24, 610–622.

Dittmar, T., Hertkorn, N., Kattner, G., and Lara, R. J. (2006). Mangroves, a major source of dissolved organic carbon to the oceans. *Global biogeochem. cycles* 20, doi: 10.1016/j.scitotenv.2017.11.225

Dittmar, T., Koch, B., Hertkorn, N., and Kattner, G. (2008). A simple and efficient method for the solid-phase extraction of dissolved organic matter (SPE-DOM) from seawater. *Limnol. Oceanogr. Methods* 6, 230–235. doi: 10.4319/lom.2008.6.230

Dittmar, T., and Lara, R. J. (2001). Do mangroves rather than rivers provide nutrients to coastal environments south of the Amazon River? Evidence from long-term flux measurements. *Mar. Ecol. Prog. Ser.* 213, 67–77. doi: 10.3354/meps213067

Dittmar, T., Lara, R. J., and Kattner, G. (2001). River or mangrove? Tracing major organic matter sources in tropical Brazilian coastal waters. *Mar. Chem.* 73, 253–271. doi: 10.1016/s0304-4203(00)00110-9

Donat, J. R., and Bruland, K. W. (1995). "Trace elements in the oceans," in *Trace Elements in Natural Waters*, eds E. Steinnes and B. Salbu (Boca Raton, FL: CRC Press), 247–281.

e Silva, C. R., Da Silva, A., and De Oliveira, S. (2006). Concentration, stock and transport rate of heavy metals in a tropical red mangrove, Natal, Brazil. *Mar. Chem.* 99, 2–11. doi: 10.1016/j.marchem.2005.09.010

Fitzpatrick, R., Powell, B., and Marvanek, S. (2008). "Atlas of Australian acid sulfate soils," in *Inland acid Sulfate Soil Systems Across Australia*, eds R. Fitzpatrick and P. Shand (Perth: CRC LEME), 75–89. CRC LEME Open File Report. No. 249.

Froelich, P. N., Klinkhammer, G., Bender, M. A. A., Luedtke, N., Heath, G. R., Cullen, D., et al. (1979). Early oxidation of organic matter in pelagic sediments of the eastern equatorial Atlantic: suboxic diagenesis. *Geochim. Cosmochim. Acta* 43, 1075–1090. doi: 10.1016/0016-7037(79)90095-4

Fry, B. (2002). Conservative mixing of stable isotopes across estuarine salinity gradients: a conceptual framework for monitoring watershed influences on downstream fisheries production. *Estuaries* 25, 264–271. doi: 10.1007/bf02691313

GeoLINK (2013). *Coffs Creek Estuary Coastal Zone Management Plan – Estuary Condition Study Report. Prepared for Coffs Harbour City Council and NSW Office of Environment and Heritage*. Coffs Harbour, NSW: GeoLINK.

Gomez-Saez, G. V., Niggemann, J., Dittmar, T., Pohlabeln, A. M., Lang, S. Q., Noowong, A., et al. (2016). Molecular evidence for abiotic sulfurization of dissolved organic matter in marine shallow hydrothermal systems. *Geochim. Cosmochim. Acta* 190, 35–52. doi: 10.1016/j.gca.2016.06.027

Gonneea, M. E., Morris, P. J., Dulaiova, H., and Charette, M. A. (2008). New perspectives on radium behavior within a subterranean estuary. *Mar. Chem.* 109, 250–267. doi: 10.1016/j.marchem.2007.12.002

Gonsior, M., Peake, B. M., Cooper, W. T., Podgorski, D., D'Andrilli, J., and Cooper, W. J. (2009). Photochemically induced changes in dissolved organic matter identified by ultrahigh resolution fourier transform ion cyclotron resonance mass spectrometry. *Environ. Sci. Technol.* 43, 698–703. doi: 10.1021/es8022804

Gonsior, M., Peake, B. M., Cooper, W. T., Podgorski, D. C., D'Andrilli, J., Dittmar, T., et al. (2011). Characterization of dissolved organic matter across the

Subtropical Convergence off the South Island. *N. Z. Mar. Chem.* 123, 99–110. doi: 10.1016/j.marchem.2010.10.004

Green, N. W., Perdue, E. M., Aiken, G. R., Butler, K. D., Chen, H., Dittmar, T., et al. (2014). An intercomparison of three methods for the large-scale isolation of oceanic dissolved organic matter. *Mar. Chem.* 161, 14–19. doi: 10.1016/j.marchem.2014.01.012

Hanor, J. S., and Chan, L.-H. (1977). Non-conservative behavior of barium during mixing of Mississippi River and Gulf of Mexico waters. *Earth Planet. Sci. Lett.* 37, 242–250. doi: 10.1016/0012-821x(77)90169-8

Hansell, D. A., and Carlson, C. A. (2014). *Biogeochemistry of Marine Dissolved Organic Matter*. Cambridge, MA: Academic Press.

Hansell, D. A., Carlson, C. A., Repeta, D. J., and Schlitzer, R. (2009). Dissolved organic matter in the ocean: a controversy stimulates new insights. *Oceanography* 22, 202–211. doi: 10.5670/oceanog.2009.109

Ho, D. T., Ferrón, S., Engel, V. C., Anderson, W. T., Swart, P. K., Price, R. M., et al. (2017). Dissolved carbon biogeochemistry and export in mangrove-dominated rivers of the Florida Everglades. *Biogeosciences* 14, 2543–2559. doi: 10.5194/bg-14-2543-2017

Holloway, C. J., Santos, I. R., Tait, D. R., Sanders, C. J., Rose, A. L., Schnetger, B., et al. (2016). Manganese and iron release from mangrove porewaters: a significant component of oceanic budgets? *Mar. Chem.* 184, 43–52. doi: 10.1016/j.marchem.2016.05.013

Jeffrey, L. C., Maher, D. T., Santos, I. R., Call, M., Reading, M. J., Holloway, C., et al. (2018). The spatial and temporal drivers of pCO_2, pCH_4 and gas transfer velocity within a subtropical estuary. *Estuar. Coastal Shelf Sci.* 208, 83–95. doi: 10.1016/j.ecss.2018.04.022

Kaul, L. W., and Froelich, P. N. (1984). Modeling estuarine nutrient geochemistry in a simple system. *Geochim. cosmochim. Acta* 48, 1417–1433. doi: 10.1016/0016-7037(84)90399-5

Kennish, M. J. (1991). *Ecology of Estuaries: Anthropogenic Effects*. Boca Raton, FA: CRC press.

Kim, S., Kramer, R. W., and Hatcher, P. G. (2003). Graphical method for analysis of ultrahigh-resolution broadband mass spectra of natural organic matter, the van Krevelen diagram. *Anal. Chem.* 75, 5336–5344. doi: 10.1021/ac034415p

Koch, B., and Dittmar, T. (2006). From mass to structure: an aromaticity index for high−resolution mass data of natural organic matter. *Rapid commun. Mass Spectrom.* 20, 926–932. doi: 10.1002/rcm.2386

Koch, B., and Dittmar, T. (2016). From mass to structure: an aromaticity index for high−resolution mass data of natural organic matter. *Rapid Commun. Mass Spectrom.* 30, 250–250. doi: 10.1002/rcm.7433

Kristensen, E., Bouillon, S., Dittmar, T., and Marchand, C. (2008). Organic carbon dynamics in mangrove ecosystems: a review. *Aquatic Bot.* 89, 201–219. doi: 10.1016/j.aquabot.2007.12.005

Kujawinski, E. B., Del Vecchio, R., Blough, N. V., Klein, G. C., and Marshall, A. G. (2004). Probing molecular-level transformations of dissolved organic matter: insights on photochemical degradation and protozoan modification of DOM from electrospray ionization Fourier transform ion cyclotron resonance mass spectrometry. *Mar. Chem.* 92, 23–37. doi: 10.1016/j.marchem.2004.06.038

Lachat. (1994). *International Methods List for the QuickChem Automated Ion Analyzer*. Millwaukee, WI: Lachat Instruments.

Luther, G. W., Kostka, J. E., Church, T. M., Sulzberger, B., and Stumm, W. (1992). Seasonal iron cycling in the salt-marsh sedimentary environment: the importance of ligand complexes with Fe (II) and Fe (III) in the dissolution of Fe (III) minerals and pyrite, respectively. *Mar. chem.* 40, 81–103. doi: 10.1016/0304-4203(92)90049-g

Machiwa, J. F. (1999). Lateral fluxes of organic carbon in a mangrove forest partly contaminated with sewage wastes. *Mangroves and Salt Marshes* 3, 95–104. doi: 10.1023/A:1009979204212

Maher, D., and Eyre, B. D. (2011). Insights into estuarine benthic dissolved organic carbon (DOC) dynamics using δ^{13}C-DOC values, phospholipid fatty acids and dissolved organic nutrient fluxes. *Geochim. Cosmochim. Acta* 75, 1889–1902. doi: 10.1016/j.gca.2011.01.007

Maher, D. T., Santos, I. R., Golsby-Smith, L., Gleeson, J., and Eyre, B. D. (2013). Groundwater-derived dissolved inorganic and organic carbon exports from a mangrove tidal creek: The missing mangrove carbon sink? *Limnol. Oceanogr.* 58, 475–488. doi: 10.4319/lo.2013.58.2.0475

Marchand, C., Allenbach, M., and Lallier-Verges, E. (2011). Relationships between heavy metals distribution and organic matter cycling in mangrove sediments (Conception Bay, New Caledonia). *Geoderma* 160, 444–456. doi: 10.1016/j.geoderma.2010.10.015

McKnight, D. M., Boyer, E. W., Westerhoff, P. K., Doran, P. T., Kulbe, T., and Andersen, D. T. (2001). Spectrofluorometric characterization of dissolved organic matter for indication of precursor organic material and aromaticity. *Limnol. Oceanogr.* 46, 38–48. doi: 10.4319/lo.2001.46.1.0038

Medeiros, P. M., Seidel, M., Ward, N. D., Carpenter, E. J., Gomes, H. R., Niggemann, J., et al. (2015). Fate of the Amazon River dissolved organic matter in the tropical atlantic ocean. *Global Biogeochem. Cycles* 29, 677–690. doi: 10.1002/2015gb005115

Menditto, A., Patriarca, M., and Magnusson, B. (2007). Understanding the meaning of accuracy, trueness and precision. *Accredit. Qual. Assur.* 12, 45–47. doi: 10.1007/s00769-006-0191-z

Milford, H. (1999). *"Soil landscapes of the Coffs Harbour 1: 100 000 Sheet Report"*, Sydney: NSW Department of Land and Water Conservation.

Millward, G. E. (1995). Processes affecting trace element speciation in estuaries. *Rev. Anal.* 120, 609–614.

Minor, E. C., Swenson, M. M., Mattson, B. M., and Oyler, A. R. (2014). Structural characterization of dissolved organic matter: a review of current techniques for isolation and analysis. *Environ. Sci.: Process. Impacts* 16, 2064–2079. doi: 10.1039/c4em00062e

Moore, R. M., Burton, J. D., Williams, P. J. L., and Young, M. L. (1979). The behaviour of dissolved organic material, iron and manganese in estuarine mixing. *Geochim. Cosmochim. Acta* 43, 919–926. doi: 10.1016/0016-7037(79)90229-1

Moore, W. S. (1997). High fluxes of radium and barium from the mouth of the Ganges-Brahmaputra River during low river discharge suggest a large groundwater source. *Earth Planet. Sci. Lett.* 150, 141–150. doi: 10.1016/S0012-821X(97)00083-6

Moore, W. S. (2010). The effect of submarine groundwater discharge on the ocean. *Annu. Rev. Mar. Sci.* 2, 59–88. doi: 10.1146/annurev-marine-120308-081019

Moore, W. S., and Shaw, T. J. (2008). Fluxes and behavior of radium isotopes, barium, and uranium in seven Southeastern US rivers and estuaries. *Mar. Chem.* 108, 236–254. doi: 10.1016/j.marchem.2007.03.004

Murray, R. H., Erler, D. V., and Eyre, B. D. (2015). Nitrous oxide fluxes in estuarine environments: response to global change. *Global change Biol.* 21, 3219–3245. doi: 10.1111/gcb.12923

Officer, C. B. (1979). Discussion of the behaviour of nonconservative dissolved constituents in estuaries. *Estuar. Coast. Mar. Sci.* 9, 91–94. doi: 10.1016/0302-3524(79)90009-4

Oksanen, J., Blanchet, F. G., Kindt, R., Legendre, P., Minchin, P. R., O'hara, R., et al. (2015). *Vegan: community ecology package. R package version 2.2–1. 2015*. Available at: http://CRAN.R-project.org/packagevegan

Osterholz, H., Kirchman, D. L., Niggemann, J., and Dittmar, T. (2016). Environmental drivers of dissolved organic matter molecular composition in the Delaware estuary. *Front. Earth Sci.* 4:95.

Peterson, B., Fry, B., Hullar, M., Saupe, S., and Wright, R. (1994). The distribution and stable carbon isotopic composition of dissolved organic carbon in estuaries. *Estuaries* 17, 111–121.

Peterson, R. N., Burnett, W. C., Taniguchi, M., Chen, J., Santos, I. R., and Misra, S. (2008). Determination of transport rates in the Yellow River–Bohai Sea mixing zone via natural geochemical tracers. *Cont. Shelf Res.* 28, 2700–2707. doi: 10.1016/j.csr.2008.09.002

Pohlabeln, A. M., Gomez-Saez, G. V., Noriega-Ortega, B. E., and Dittmar, T. (2017). Experimental evidence for abiotic sulfurization of marine dissolved organic matter. *Front. Mar. Sci.* 4:364.

R Core Team (2016). *R: A language and environment for statistical computing*. Vienna, Austria: R Foundation for Statistical Computing. Available online at: http://www.R-project.org/

Ramette, A. (2007). Multivariate analyses in microbial ecology. *FEMS Microbiol. Ecol.* 62, 142–160. doi: 10.1111/j.1574-6941.2007.00375.x

Ray, R., Baum, A., Rixen, T., Gleixner, G., and Jana, T. (2018). Exportation of dissolved (inorganic and organic) and particulate carbon from mangroves and its implication to the carbon budget in the Indian Sundarbans. *Sci. Total Environ.* 621, 535–547. doi: 10.1016/j.scitotenv.2017.11.225

Raymond, P. A., and Bauer, J. E. (2001a). DOC cycling in a temperate estuary: a mass balance approach using natural ^{14}C and ^{13}C isotopes. *Limnol. Oceanogr.* 46, 655–667. doi: 10.4319/lo.2001.46.3.0655

Raymond, P. A., and Bauer, J. E. (2001b). Use of ^{14}C and ^{13}C natural abundances for evaluating riverine, estuarine, and coastal DOC and POC sources and cycling: a review and synthesis. *Org. Geochem.* 32, 469–485. doi: 10.1016/S0146-6380(00)00190-X

Raymond, P. A., Saiers, J. E., and Sobczak, W. V. (2016). Hydrological and biogeochemical controls on watershed dissolved organic matter transport: Pulse-shunt concept. *Ecology* 97, 5–16. doi: 10.1890/14-1684.1

Reading, M. J., Santos, I. R., Maher, D. T., Jeffrey, L. C., and Tait, D. R. (2017). Shifting nitrous oxide source/sink behaviour in a subtropical estuary revealed by automated time series observations. *Estuar. Coast. Shelf Sci.* 194, 66–76. doi: 10.1016/j.ecss.2017.05.017

Reddy, K. R., and DeLaune, R. D. (2008). *Biogeochemistry of Wetlands: Science and Applications*. Boca Raton, FA: CRC press.

Romigh, M. M., Davis, S. E., Rivera-Monroy, V. H., and Twilley, R. R. (2006). Flux of organic carbon in a riverine mangrove wetland in the Florida Coastal Everglades. *Hydrobiologia* 569, 505–516. doi: 10.1007/s10750-006-0152-x

Roper, T., Creese, B., Scanes, P., Stephens, K., Williams, R., Dela-Cruz, J., et al. (2011). *Assessing the Condition of Estuaries and Coastal lake Ecosystems in NSW*. Hurstville, AS: Office of Environment and Heritage.

Rossel, P. E., Vähätalo, A. V., Witt, M., and Dittmar, T. (2013). Molecular composition of dissolved organic matter from a wetland plant (*Juncus effusus*) after photochemical and microbial decomposition (1.25 yr): common features with deep sea dissolved organic matter. *Org. Geochem.* 60, 62–71. doi: 10.1016/j.orggeochem.2013.04.013

Sadat-Noori, M., Santos, I. R., Tait, D. R., Reading, M. J., and Sanders, C. J. (2017). High porewater exchange in a mangrove-dominated estuary revealed from short-lived radium isotopes. *J. Hydrol.* 553, 188–198. doi: 10.1016/j.jhydrol.2017.07.058

Samanta, S., and Dalai, T. K. (2016). Dissolved and particulate barium in the Ganga (Hooghly) River estuary, India: solute-particle interactions and the enhanced dissolved flux to the oceans. *Geochim. Cosmochim. Acta* 195, 1–28. doi: 10.1016/j.gca.2016.09.005

Sanders, C. J., Santos, I. R., Maher, D. T., Sadat-Noori, M., Schnetger, B., and Brumsack, H. -J. (2015). Dissolved iron exports from an estuary surrounded by coastal wetlands: can small estuaries be a significant source of Fe to the ocean? *Mar. Chem.* 176, 75-82. doi: 10.1016/j.marchem.2015.07.009

Santos, I. R., Bryan, K. R., Pilditch, C. A., and Tait, D. R. (2014). Influence of porewater exchange on nutrient dynamics in two New Zealand estuarine intertidal flats. *Mar. Chem.* 167, 57–70. doi: 10.1016/j.marchem.2014.04.006

Santos, I. R., Burnett, W. C., Dittmar, T., Suryaputra, I. G., and Chanton, J. (2009). Tidal pumping drives nutrient and dissolved organic matter dynamics in a Gulf of Mexico subterranean estuary. *Geochim. Cosmochim. Acta* 73, 1325-1339. doi: 10.1016/j.gca.2008.11.029

Santos, I. R., Burnett, W. C., Misra, S., Suryaputra, I. G. N. A., Chanton, J. P., Dittmar, T., et al. (2011a). Uranium and barium cycling in a salt wedge subterranean estuary: the influence of tidal pumping. *Chem. Geol.* 287, 114-123. doi: 10.1016/j.chemgeo.2011.06.005

Santos, I. R., De Weys, J., and Eyre, B. D. (2011b). Groundwater or floodwater? assessing the pathways of metal exports from a coastal acid sulfate soil catchment. *Environ. Sci. Technol.* 45, 9641–9648. doi: 10.1021/es202581h

Schlitzer, R. (2002). Interactive analysis and visualization of geoscience data with ocean data view. *Comput. Geosci.* 28, 1211–1218. doi: 10.1016/s0098-3004(02)00040-7

Schmidt, F., Elvert, M., Koch, B., Witt, M., and Hinrichs, K. -U. (2009). Molecular characterization of dissolved organic matter in pore water of continental shelf sediments. *Geochim. Cosmochim. Acta* 73, 3337–3358. doi: 10.1016/j.gca.2009.03.008

Schmidt, M. W., Torn, M. S., Abiven, S., Dittmar, T., Guggenberger, G., Janssens, I. A., et al. (2011). Soil organic matter persistence as an ecosystem property. *Nature* 478, 49–56. doi: 10.1038/nature10386

Seidel, M., Beck, M., Riedel, T., Waska, H., Suryaputra, I. G., Schnetger, B., et al. (2014). Biogeochemistry of dissolved organic matter in an anoxic intertidal creek bank. *Geochim. Cosmochim. Acta* 140, 418–434. doi: 10.1016/j.gca.2014.05.038

Seidel, M., Manecki, M., Herlemann, D. P. R., Deutsch, B., Schulz-Bull, D., Jürgens, K., et al. (2017). Composition and transformation of dissolved organic matter in the Baltic Sea. *Front Earth Sci.* 5:31. doi: 10.3389/feart.2017.00031

Seidel, M., Yager, P. L., Ward, N. D., Carpenter, E. J., Gomes, H. R., Krusche, A. V., et al. (2015). Molecular-level changes of dissolved organic matter along the Amazon River-to-ocean continuum. *Mar. Chem.* 177, 218–231. doi: 10.1016/j.marchem.2015.06.019

Shaw, T.J., Moore, W.S., Kloepfer, J., and Sochaski, M.A. (1998). The flux of barium to the coastal waters of the southeastern USA: the importance of submarine groundwater discharge. *Geochim. Cosmochim. Acta* 62, 3047-3054. doi: 10.1016/S0016-7037(98)00218-X

Sholkovitz, E.R. (1978). The flocculation of dissolved Fe, Mn, Al, Cu, Ni, Co and Cd during estuarine mixing. *Earth Planet. Sci. Lett.* 41, 77-86. doi: 10.1016/0012-821X(78)90043-2

Singh, S. P., Singh, S. K., and Bhushan, R. (2013). Internal cycling of dissolved barium in water column of the Bay of Bengal. *Mar. Chem.* 154, 12–23. doi: 10.1016/j.marchem.2013.04.013

Sippo, J. Z., Maher, D. T., Tait, D. R., Holloway, C., and Santos, I. R. (2016). Are mangroves drivers or buffers of coastal acidification? Insights from alkalinity and dissolved inorganic carbon export estimates across a latitudinal transect. *Global Biogeochem. Cycles* 30, 753–766. doi: 10.1002/2015gb005324

Sippo, J. Z., Maher, D. T., Tait, D. R., Ruiz-Halpern, S., Sanders, C. J., and Santos, I. R. (2017). Mangrove outwelling is a significant source of oceanic exchangeable organic carbon. *Limnol. Oceanogr. Lett.* 2, 1–8. doi: 10.1002/lol2.10031

Sleighter, R., and Hatcher, P. (2008). Molecular characterization of dissolved organic matter (DOM) along a river to ocean transect of the lower Chesapeake Bay by ultrahigh resolution electrospray ionization fourier transform ion cyclotron resonance mass spectrometry *Mar. Chem.* 110, 140–152.

Sleighter, R. L., Chin, Y. -P., Arnold, W. A., Hatcher, P. G., McCabe, A. J., McAdams, B. C., et al. (2014). Evidence of incorporation of abiotic S and N into prairie wetland dissolved organic matter. *Environ. Sci. Technol. Lett.* 1, 345-350. doi: 10.1021/ez500229b

Spiker, E. (1980). The behavior of ^{14}C and ^{13}C in estuarine water; effects of *in situ* CO_2 production and atmospheric change. *Radiocarbon* 22, 647–654. doi: 10.1017/s0033822200010018

St-Jean, G. (2003). Automated quantitative and isotopic (^{13}C) analysis of dissolved inorganic carbon and dissolved organic carbon in continuous-flow using a total organic carbon analyser. *Rapid commun. Mass Spectrom.* 17, 419-428. doi: 10.1002/rcm.926

Stecher, H. A., and Kogut, M. B. (1999). Rapid barium removal in the Delaware estuary. *Geochim. Cosmochim. Acta* 63, 1003-1012. doi: 10.1016/S0016-7037(98)00310-X

Sunda, W. G. (1989). Trace metal interactions with marine phytoplankton. *Biol. Oceanogr.* 6, 411–442.

Sunda, W. G. (2000). "Trace metal-phytoplankton interactions in aquatic systems," in *Environmental Microbe-Metal Interactions*, ed. D. R. Lovley (Washington, DC: American Society of Microbiology).

Taillardat, P., Willemsen, P., Marchand, C., Friess, D. A. Widory, D., Baudron, P., et al. (2018). Assessing the contribution of porewater discharge in carbon export and CO_2 evasion in a mangrove tidal creek (Can Gio, Vietnam). *J. Hydrol.* 563, 303–318 doi: 10.1016/j.jhydrol.2018.05.042

Thurman, E. M. (2012). *Organic Geochemistry of Natural Waters*. Berlin: Springer Science & Business Media.

Tremblay, L. B., Dittmar, T., Marshall, A. G., Cooper, W. J., and Cooper, W. T. (2007). Molecular characterization of dissolved organic matter in a North Brazilian mangrove porewater and mangrove-fringed estuaries by ultrahigh resolution fourier transform-ion cyclotron resonance mass spectrometry and excitation/emission spectroscopy. *Mar. Chem.* 105, 15–29. doi: 10.1016/j.marchem.2006.12.015

Twilley, R. R. (1985). The exchange of organic carbon in basin mangrove forests in a southwest Florida estuary. *Estuar. Coast. Shelf Sci.* 20, 543–557. doi: 10.1016/0272-7714(85)90106-4

van Krevelen, D. W. (1950). Graphical-statistical method for the study of structure and reaction processes of coal. *Fuel* 29, 269–284.

Ward, N. D., Keil, R. G., Medeiros, P. M., Brito, D. C., Cunha, A. C., Dittmar, T., et al. (2013). Degradation of terrestrially derived macromolecules in the Amazon River. *Nat. Geosci.* 6, 530. doi: 10.1038/ngeo1817

Water Technology (2013). *Coffs Creek infilling and hydraulic study, Report prepared for Coffs Harbour City Council*. Coffs Harbour, NSW: Coffs Harbour City Council.

Wong, W. W., Grace, M. R., Cartwright, I., Cardenas, M. B., Zamora, P. B., and Cook, P. L. (2013). Dynamics of groundwater-derived nitrate and nitrous oxide in a tidal estuary from radon mass balance modeling. *Limnol. Oceanogr.* 58, 1689–1706. doi: 10.4319/lo.2013.58.5.1689

Zark, M., Christoffers, J., and Dittmar, T. (2017). Molecular properties of deep-sea dissolved organic matter are predictable by the central limit theorem: evidence from tandem FT-ICR-MS. *Mar. Chem.* 191, 9–15. doi: 10.1016/j.marchem.2017.02.005

Conflict of Interest Statement: The authors declare that the research was conducted in the absence of any commercial or financial relationships that could be construed as a potential conflict of interest.